



## OPEN ACCESS

## EDITED BY

Sanjeev Kumar,  
Physical Research Laboratory, India

## REVIEWED BY

Damian L. Arévalo-Martínez,  
Radboud University, Netherlands  
Sohiko Kameyama,  
Hokkaido University, Japan

## \*CORRESPONDENCE

Annie Bourbonnais  
✉ [abourbonnais@seoe.sc.edu](mailto:abourbonnais@seoe.sc.edu)

RECEIVED 03 January 2023

ACCEPTED 31 March 2023

PUBLISHED 12 May 2023

## CITATION

Bourbonnais A, Chang BX, Sonnerup RE,  
Doney SC and Altabet MA (2023) Marine  
N<sub>2</sub>O cycling from high spatial resolution  
concentration, stable isotopic and  
isotopomer measurements along a  
meridional transect in the eastern  
Pacific Ocean.

*Front. Mar. Sci.* 10:1137064.

doi: 10.3389/fmars.2023.1137064

## COPYRIGHT

© 2023 Bourbonnais, Chang, Sonnerup,  
Doney and Altabet. This is an open-access  
article distributed under the terms of the  
[Creative Commons Attribution License  
\(CC BY\)](https://creativecommons.org/licenses/by/4.0/). The use, distribution or  
reproduction in other forums is permitted,  
provided the original author(s) and the  
copyright owner(s) are credited and that  
the original publication in this journal is  
cited, in accordance with accepted  
academic practice. No use, distribution or  
reproduction is permitted which does not  
comply with these terms.

# Marine N<sub>2</sub>O cycling from high spatial resolution concentration, stable isotopic and isotopomer measurements along a meridional transect in the eastern Pacific Ocean

Annie Bourbonnais<sup>1\*</sup>, Bonnie X. Chang<sup>2</sup>, Rolf E. Sonnerup<sup>2</sup>,  
Scott C. Doney<sup>3</sup> and Mark A. Altabet<sup>4</sup>

<sup>1</sup>School of the Earth, Ocean and Environment, University of South Carolina, Columbia, SC, United States, <sup>2</sup>Cooperative Institute for Climate, Ocean, and Ecosystem Studies, University of Washington, Seattle, WA, United States, <sup>3</sup>Department of Environmental Sciences, University of Virginia, Charlottesville, VA, United States, <sup>4</sup>School for Marine Science and Technology, University of Massachusetts, Dartmouth, MA, United States

Nitrous oxide (N<sub>2</sub>O) is a potent greenhouse gas and ozone depleting substance, with the ocean accounting for about one third of global emissions. In marine environments, a significant amount of N<sub>2</sub>O is produced by biological processes in Oxygen Deficient Zones (ODZs). While recent technological advances are making surface N<sub>2</sub>O concentration more available, high temporal and spatial resolution water-column N<sub>2</sub>O concentration data are relatively scarce, limiting global N<sub>2</sub>O ocean models' predictive capability. We present a N<sub>2</sub>O concentration, stable isotopic composition and isotopomer dataset of unprecedentedly large spatial coverage and depth resolution in the broader Pacific, crossing both the eastern tropical South and North Pacific Ocean ODZs collected as part of the GO-SHIP P18 repeat hydrography program in 2016/2017. We complement these data with dissolved gases (nitrogen, oxygen, argon) and nitrate isotope data to investigate the pathways controlling N<sub>2</sub>O production in relation to apparent oxygen utilization and fixed nitrogen loss. N<sub>2</sub>O yield significantly increased under low oxygen conditions near the ODZs. Keeling plot analysis revealed different N<sub>2</sub>O sources above the ODZs under different oxygen regimes. Our stable isotopic data and relationships between the N<sub>2</sub>O added by microbial processes ( $\Delta N_2O$ ) and dissolved inorganic nitrogen (DIN) deficit confirm increased N<sub>2</sub>O production by denitrification under low oxygen conditions near the oxycline where the largest N<sub>2</sub>O accumulations were observed. The slope for  $\delta^{18}O-N_2O$  versus site preference (SP, the difference between the central ( $\alpha$ ) and outer ( $\beta$ ) N atoms in the linear N<sub>2</sub>O molecule) in the eastern tropical North Pacific ODZ was lower than expected for pure N<sub>2</sub>O reduction, likely because of the observed decrease in  $\delta^{15}N^{\beta}$ . This trend is consistent with prior ODZ studies and attributed to concurrent production of N<sub>2</sub>O from nitrite with a low  $\delta^{15}N$  or denitrification with a SP >0%. We estimated

apparent isotope effects for  $\text{N}_2\text{O}$  consumption in the ETNP ODZ of 3.6‰ for  $^{15}\text{N}^{\text{bulk}}$ , 9.4‰ for  $^{15}\text{N}^{\alpha}$ , -2.3‰ for  $^{15}\text{N}^{\beta}$ , 12.0‰ for  $^{18}\text{O}$ , and 11.7‰ for SP. These values were generally within ranges previously reported for previous laboratory and field experiments.

#### KEYWORDS

nitrous oxide, greenhouse gas, stable isotopes, isotopomers, oxygen deficient zones, eastern South Pacific Ocean, eastern North Pacific Ocean, Southern Ocean

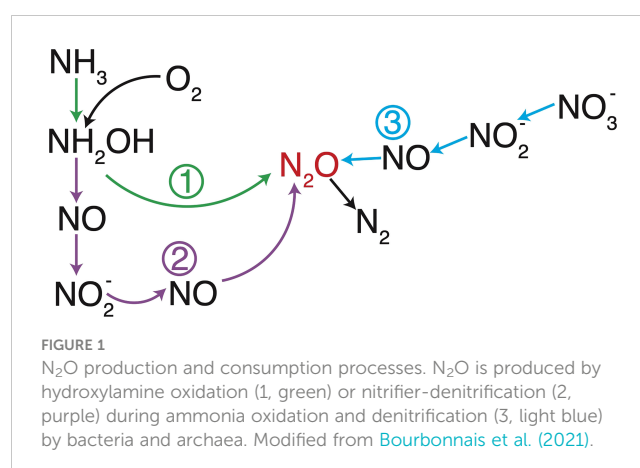
## 1 Introduction

Nitrous oxide ( $\text{N}_2\text{O}$ ) is mainly produced by microbial processes and contributes to climate change as a tropospheric greenhouse gas approximately 275 times more potent than  $\text{CO}_2$  on a per molecule basis (Forster et al., 2021).  $\text{N}_2\text{O}$  produced at the Earth's surface has a long atmospheric residence time of more than 100 years and is the main source of ozone-depleting nitric-oxide radicals in the stratosphere (Nevison and Holland, 1997; Ravishankara et al., 2009). Biogeochemical models estimate that the ocean accounts for about one third of global  $\text{N}_2\text{O}$  emissions (Freing et al., 2012; Ciais et al., 2013; Tian et al., 2020; Forster et al., 2021) with a global oceanic flux estimate of  $4.2 \pm 1.0 \text{ Tg N y}^{-1}$  (Yang et al., 2020). Coastal upwelling systems associated with Oxygen Deficient Zones (ODZs) account for up to 35% of the oceanic  $\text{N}_2\text{O}$  total emissions (Bakker et al., 2014; Arévalo-Martínez et al., 2015; Yang et al., 2020), yet temporal variability from these productive coastal waters is still not well quantified.

$\text{N}_2\text{O}$  is produced in oxic ocean waters as a by-product of nitrification through the oxidation of hydroxylamine ( $\text{NH}_2\text{OH}$ ), an intermediate during ammonia ( $\text{NH}_3$ ) oxidation to nitrite ( $\text{NO}_2^-$ ) by both archaeal and bacterial nitrifiers (Caranto and Lancaster, 2017) (Figure 1). Under low oxygen ( $\text{O}_2$ )-conditions, ammonia oxidizing bacteria (AOB) produce  $\text{N}_2\text{O}$  by nitrifier-denitrification, the sequential  $\text{NO}_2^-$  reduction to  $\text{N}_2\text{O}$  during respiration (Goreau et al., 1980; Wrage et al., 2001; Frame and Casciotti, 2010).  $\text{N}_2\text{O}$  is also produced by ammonia oxidizing archaea (AOA) following a hybrid pathway where one atom in the  $\text{N}_2\text{O}$  molecule is derived from  $\text{NH}_3$  (e.g.,  $\text{NH}_2\text{OH}$ ) and the other from  $\text{NO}_2^-$  (Trimmer et al., 2016).  $\text{N}_2\text{O}$  production by nitrification leads to strong positive correlations between Apparent Oxygen Utilization (AOU) and  $\Delta\text{N}_2\text{O}$  (i.e., the difference between  $\text{N}_2\text{O}$  measured and at atmospheric equilibrium) and nitrate ( $\text{NO}_3^-$ ) concentrations (Yoshinari and Knowles, 1976; Cohen and Gordon, 1979; Nevison et al., 2003).  $\text{N}_2\text{O}$  production yield per  $\text{NO}_2^-$  generated during nitrification by either AOA or AOB is generally low, varying from 0 to 2% of  $\text{NO}_3^-$  production (Yoshida et al., 1989; Frame and Casciotti, 2010; Santoro et al., 2010; Santoro et al., 2011; Löscher et al., 2012; Ryabenko et al., 2012) but is generally higher for AOB (Hink et al., 2017a; Hink et al., 2017b) and enhanced under low- $\text{O}_2$  conditions according to both culture and field observations (up to 10% at low  $\text{O}_2$ ; Goreau et al., 1980; Ji et al., 2015).

Under anoxic conditions, denitrification, the sequential reduction of  $\text{NO}_3^-$ ,  $\text{NO}_2^-$ , and  $\text{NO}$  to  $\text{N}_2\text{O}$ , both produces and consumes  $\text{N}_2\text{O}$ . Enhanced  $\text{N}_2\text{O}$  production occurs under low- $\text{O}_2$  conditions (generally below  $10 \mu\text{mol kg}^{-1}$ ; Frey et al., 2020) due to different  $\text{O}_2$  sensitivities for the different steps involved in denitrification, with nitrous oxide reductase being inhibited by even nanomolar  $\text{O}_2$  concentrations (Dalsgaard et al., 2014).  $\text{N}_2\text{O}$  produced by incomplete denitrification significantly accumulates in low- $\text{O}_2$  conditions near the upper oxycline in the eastern tropical North Pacific (ETNP) and eastern tropical South Pacific (ETSP) ODZs (e.g., Ji et al., 2015; Kock et al., 2016; Bourbonnais et al., 2017; Casciotti et al., 2018; Frey et al., 2020; Kelly et al., 2021; Monreal et al., 2022). High  $\text{N}_2\text{O}$  accumulations of up to  $1 \mu\text{mol L}^{-1}$  were observed in surface waters off the Peru coast, where anoxic waters from the ETSP ODZ are continuously upwelled (Arévalo-Martínez et al., 2015).  $\text{N}_2\text{O}$  accumulation is caused by a decoupling between  $\text{N}_2\text{O}$  production and its reduction to  $\text{N}_2$  by denitrification, the latter process being less  $\text{O}_2$  tolerant (Dalsgaard et al., 2014).  $\text{N}_2\text{O}$  is generally completely reduced to non-bioavailable  $\text{N}_2$  in anoxic waters. ODZs are thus generally net  $\text{N}_2\text{O}$  sinks, with concentrations near or below atmospheric equilibrium concentrations (Bange et al., 2001; Yamagishi et al., 2007; Kock et al., 2016).

Natural stable isotopes are broadly used as tracers of N-cycle processes in the ocean which integrate over space and time (e.g., Sigman et al., 2005; Altabet, 2006; Bourbonnais et al., 2009;



Bourbonnais et al., 2015). The  $N_2O$  molecule contains both bulk ( $\delta^{15}N$  and  $\delta^{18}O$ ) and, given its asymmetric arrangement of atoms,  $^{15}N$  site specific signatures that are valuable for identifying production and consumption processes. Bulk  $\delta^{15}N$  and  $\delta^{18}O$  are expressed as:

$$\delta^{15}N \text{ or } \delta^{18}O = ((R_{\text{sample}}/R_{\text{reference}} - 1) \times 1000 \quad (\text{eq. 1})$$

Units are in parts per thousand or per mil (‰) and R is the ratio of  $^{15}N/^{14}N$  or  $^{18}O/^{16}O$ . Reference materials are atmospheric  $N_2$  for N (scale AIR- $N_2$ ) and mean ocean water for O (scale Vienna Standard Mean Ocean Water, V-SMOW). The bulk isotopic composition ( $\delta^{15}N$  and  $\delta^{18}O$ ) of  $N_2O$  depends in part on the isotopic composition of its substrates. For instance, for hydroxylamine oxidation, bulk  $N_2O$   $\delta^{15}N$  and  $\delta^{18}O$  depend on the  $\delta^{15}N$  of the source  $NH_3$  and  $\delta^{18}O$  of dissolved  $O_2$ . Conversely for nitrifier-denitrification and denitrification,  $N_2O$   $\delta^{15}N$  and  $\delta^{18}O$  is dependent on the  $\delta^{15}N$  and  $\delta^{18}O$  of source  $NO_3^-$  and/or  $NO_2^-$  (Ostrom and Ostrom, 2012). Additionally, significant O exchange usually occurs between  $NO_2^-$  and  $H_2O$  during  $N_2O$  production by nitrifier-denitrification or denitrification (Buchwald and Casciotti, 2010; Kool et al., 2011), which acts to decouple the  $\delta^{18}O$  values of source and product.

Isotopic fractionation during nitrification and denitrification is the other major influence on the  $\delta^{15}N$  and  $\delta^{18}O$  of  $N_2O$ . Kinetic isotope fractionation occurs as the molecules containing the lighter isotopes (e.g.,  $^{14}N$ ,  $^{16}O$ ) react more quickly leaving the residual substrate enriched in heavier isotopes (e.g.,  $^{15}N$  and  $^{18}O$ ). The isotope effect ( $\epsilon$ ) is defined by:

$$\epsilon(\text{‰}) = ((k_2/k_1) - 1) \times 1000 \quad (\text{eq. 2})$$

where  $k_1$  and  $k_2$  are the specific reaction rates for the lighter and heavier isotope, respectively. N and O isotope effects ( $^{15}\epsilon$ ,  $^{18}\epsilon$ ) during  $N_2O$  production and consumption vary substantially in laboratory culture as well as in the environment (Bourbonnais et al., 2017 and references therein).

In contrast to bulk isotope values,  $N_2O$  Site Preference (SP) is independent of initial isotopic composition of the substrate (Toyoda et al., 2002; Schmidt et al., 2004; Sutka et al., 2006). Thus, SP is generally process-dependent and can be used as a tracer to identify the source of  $N_2O$ . SP is calculated from the difference in  $\delta^{15}N$  between the central ( $\alpha$ ) and outer ( $\beta$ ) N atoms in the linear, asymmetrical  $N_2O$  molecule (NNO):

$$SP = \delta^{15}N^{\alpha} - \delta^{15}N^{\beta} \quad (\text{eq. 3})$$

Non-zero SP arises from the differential biochemical bond making and breaking experienced by each of the two N atoms as a consequence of their different molecular positions. Low SP isotopic signatures (-11 to 0‰) are associated with  $N_2O$  production via  $NO_2^-$  reduction by nitrifier-denitrification or denitrification. Much higher SP values are indicative of abiotic  $N_2O$  formation (Heil et al., 2014) or production by hydroxylamine oxidation (30-36‰) (Sutka et al., 2006; Frame and Casciotti, 2010).  $N_2O$  isotopic signatures have consequently been classified into distinct compositional fields used to evaluate the relative contribution from different processes (e.g., Wankel et al., 2017

and reference therein). However, SP does increase as a result of isotope fractionation during consumption by denitrification as discussed above (Yamagishi et al., 2005; Ostrom et al., 2007; Yamagishi et al., 2007).

The main objectives of this study are to better understand nitrous oxide ( $N_2O$ ) distribution and production mechanisms along the meridional P18 transect in the eastern Pacific sampled as part of the U.S. GO-SHIP program (Figure 2). We sampled at an unprecedentedly high spatial resolution to investigate how  $N_2O$  dynamics respond to changes in  $O_2$  concentrations and dissolved inorganic nitrogen (DIN) loss. We then evaluated pathways responsible for  $N_2O$  production in sub-oxic waters ( $O_2 > 5 \mu\text{mol kg}^{-1}$ ) overlying the ETNP and ETSP ODZs as well as deep waters using stable isotopes and isotopomers and Keeling plot analysis. We also investigated  $N_2O$  cycling within the ETNP ODZ and estimated apparent isotope effects for  $N_2O$  consumption.

## 2 Methods

The U.S. GO-SHIP Program conducted a hydrographic survey along the P18 section in 2016/2017 (Figure 2). Core physical and biogeochemical data from the cruise (e.g., temperature and salinity,  $O_2$  and nutrient concentrations, transient tracers, radiocarbon) are publicly available at <https://cchdo.ucsd.edu/cruise/33RO20161119>. Samples for  $N_2/Ar$  were collected every ~2 degrees latitude during leg 1 at 25 stations in total.  $N_2O$  stable isotope and isotopomer samples were collected at 44 stations, every ~2 degrees latitude during leg 1 and every 3 to 4 degrees during leg 2, except between 3°

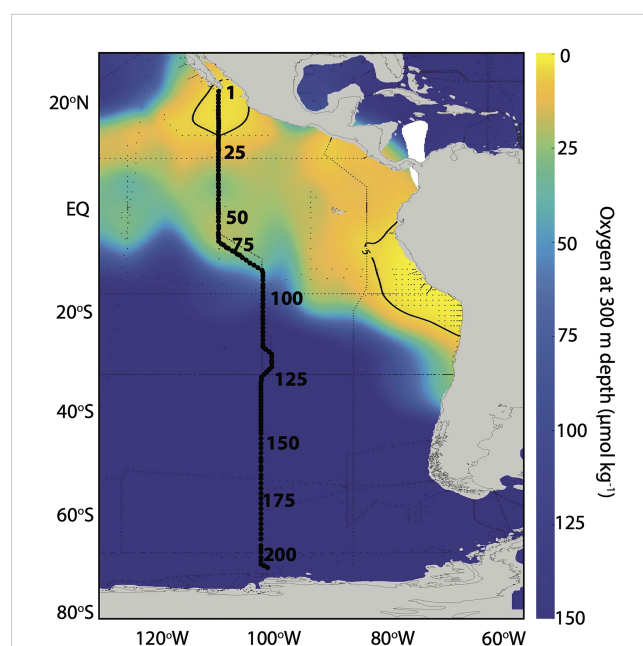


FIGURE 2  
Stations sampled as part of the U.S. GO-SHIP Program along the P18 section in 2016/2017. Representative station numbers (every 25 stations) are shown along the transect. Colors indicate  $O_2$  concentration at 300 m depth from the Global Ocean Data Analysis Project (GLODAPv2.2022). The  $5 \mu\text{mol kg}^{-1} O_2$  contour is shown.

N and  $^3\text{S}$  where the resolution was increased to  $\sim 1$  degree. Samples for  $\delta^{15}\text{N}$  of  $\text{NO}_3^-$  analysis were collected during leg 1 at every degree of latitude, but only analyzed at station 32 in the ETNP and stations 53, 55, 62, 68, 74, 78, 90, 92, 96, 100, 104, 108 and 112 near the equator and the ETNP. We usually collected water column profiles from the surface to 2000 m depth, with deeper profiles at 3 stations.

## 2.1 $\text{N}_2/\text{Ar}$

$\text{N}_2/\text{Ar}$  and  $\delta^{15}\text{N}_2$  samples were collected and preserved as in Charoenpong et al. (2014) and analyzed at the University of Massachusetts Dartmouth (UMass Dartmouth). In total, approximately 600 samples were collected in 60 mL serum bottles. Water samples were pumped, at 5 to 10 ml  $\text{min}^{-1}$ , through a continuous sparger which transfers dissolved gases quantitatively to a continuous flow of helium (He) carrier gas. Analysis time was about 10 minutes. Carrier gas was passed through water, carbon dioxide ( $\text{CO}_2$ ), and software selectable hot-copper  $\text{O}_2$  traps before admittance *via* an open split to an isotope-ratio mass spectrometer (IRMS). The GV IsoPrime IRMS was fitted with collectors for simultaneous measurement of  $\text{N}_2$  (masses 28 and 29),  $\text{O}_2$  (masses 32, 33, and 34), and Ar (mass 40). Gas and isotopic ratios were measured against artificial compressed gas mixtures of  $\text{N}_2$ ,  $\text{O}_2$ , and Ar close to expected dissolved gas ratios. Reproducibility of  $\text{N}_2/\text{Ar}$  measurements were better than 0.5%. Daily calibration against an atmosphere reference (water equilibrated with air) was carried out at precisely controlled temperatures of 10.0 and 20.0°C. Excess (biogenic)  $\text{N}_2$  was calculated against equilibrium values expected from *in situ* temperature and salinity as in Charoenpong et al. (2014). Subtraction of the background  $\text{N}_2$  excess was done as in Bourbonnais et al. (2015) using  $\text{N}_2/\text{Ar}$  values in source waters near the equator.

## 2.2 $\text{N}_2\text{O}$ concentrations, stable isotopes and isotopomers

Samples for dissolved  $\text{N}_2\text{O}$  were collected in a similar fashion as for dissolved  $\text{O}_2/\text{N}_2/\text{Ar}$  samples. Tygon tubing was attached to the Niskin bottle and a 165 mL serum glass bottle was filled and overflowed with seawater at least 2 times before capping with a butyl stopper and crimp sealed with aluminum. This procedure was executed underwater in a plastic container to avoid air bubbles. After collection, 0.2 mL of a saturated  $\text{HgCl}_2$  solution was injected to prevent biological activity. In total, approximately 800 samples were collected.

Samples were analyzed at UMass Dartmouth using a GV IsoPrime Continuous Flow, MultiCollector, IRMS (CF-MC-IRMS) coupled to an automated gas extraction as described in Bourbonnais et al. (2017). The collector configuration included masses 30, 31 for the  $\text{NO}^+$  fragment of  $\text{N}_2\text{O}$  (used for the determination of  $\delta^{15}\text{N}^\alpha$ ) and 44, 45, and 46 (used for the determination of  $\delta^{15}\text{N}^{\text{bulk}}$  and  $\delta^{18}\text{O}$ ). Briefly, dissolved  $\text{N}_2\text{O}$  was pumped through a gas extractor, completely extracted through bubbling with a continuous flow of He and concentrated and purified in a purge-trap system.  $\text{CO}_2$  and  $\text{H}_2\text{O}$  vapor were

removed using chemical and cryogenic traps.  $\text{N}_2\text{O}$  was cryo-focused with two liquid  $\text{N}_2$  traps and passed through a capillary gas chromatography (GC) column prior to IRMS analysis. Results were reproducible even at low  $\text{N}_2\text{O}$  concentration (down to  $\sim 5$  nmol  $\text{L}^{-1}$ ).  $\text{N}_2\text{O}$  concentrations in our samples were calculated from relative peak heights between the samples and a seawater standard of known  $\text{N}_2\text{O}$  concentration equilibrated with seawater at 5°C (12.5 nmol  $\text{L}^{-1}$  at salinity 34 as calculated using the Weiss and Price (1980) equation). Equilibrium  $\text{N}_2\text{O}$  concentrations at depth were calculated using historical reconstructions of atmospheric  $\text{N}_2\text{O}$  and water mass age distributions estimated from chlorofluorocarbon and sulfur hexafluoride tracers as described in section 2.4.

The  $\text{N}_2\text{O}$  concentrations measured with our IRMS agreed well with those measured independently using gas chromatography and an electron capture detector (ECD) at sea during the same research expedition (data available at <https://cchdo.ucsd.edu/cruise/33RO20161119>).

The reproducibility of  $\delta^{15}\text{N}^{\text{bulk}}$ , the average of  $\delta^{15}\text{N}^\alpha$  and  $\delta^{15}\text{N}^\beta$ ,  $\delta^{18}\text{O}$  and SP as well as any instrumental drift were determined from measurements of the 5°C seawater standard distributed throughout an analytical run. We calibrated measurements and corrected for scrambling between the  $\alpha$  and  $\beta$  positions (Westley et al., 2007) using four  $\text{N}_2\text{O}$  standards covering a large range of SP (as well as  $\delta^{15}\text{N}^{\text{bulk}}$  and  $\delta^{18}\text{O}$ ) composition (see Mohn et al., 2014). These standards were analyzed in duplicate for each run to quantify the scrambling effect and potential offsets, and we iteratively solved for the different calibration parameters as described in Frame and Casciotti (2010) and Mohn et al. (2014). Correction for isobaric interference from  $^{17}\text{O}$  was included in these procedures. Standard deviations for triplicate measurements of our  $\text{N}_2\text{O}$  standards were typically below 0.1‰ for  $\delta^{15}\text{N}^{\text{bulk}}$   $\text{N}_2\text{O}$ , 0.1‰ for  $\delta^{18}\text{O}$ - $\text{N}_2\text{O}$  and 1.0‰ for SP, which were comparable to values reported by Mohn et al. (2014).

## 2.3 Nitrate isotopes

The  $\delta^{15}\text{N}$  of  $\text{NO}_3^-$  was measured using the Ti (III) reduction method for nitrate conversion to  $\text{N}_2\text{O}$  (Altabet et al., 2019). The product  $\text{N}_2\text{O}$  was purified and analyzed at UMass Dartmouth using a GV IsoPrime continuous flow IRMS equipped with a custom purge trap extraction system and a PAL autosampler. Target sample size was 10 nmoles. Samples were standardized using a three-point correction with the international standards IAEA-N3 ( $\delta^{15}\text{N} = 4.7\text{‰}$  vs AIR), USGS-34 ( $\delta^{15}\text{N} = -1.8\text{‰}$  vs AIR) and USGS-35 ( $2.7\text{‰}$  vs AIR). The isotope ratios are expressed in  $\delta$  (‰) relative to AIR for N. The average standard deviation for duplicate samples was better than  $\pm 0.3\text{‰}$  for  $\delta^{15}\text{N}$ .

## 2.4 Calculation of $\text{N}_2\text{O}$ at equilibrium using transit time distributions

In the same water parcel as  $\text{N}_2\text{O}$ , three transient tracers [chlorofluorocarbon (CFC)-11, CFC-12, and sulfur hexafluoride ( $\text{SF}_6$ )] were measured, each of which are affected by mixing

differently due to their differing atmospheric histories. This concurrence provides a means of estimating, from multiple tracer ages, the impact of mixing on the ages. To estimate mean ventilation timescales, age distributions, otherwise known as transit-time distributions (TTDs), were approximated using the inverse Gaussian form:

$$G(t) = \sqrt{\frac{\Gamma^3}{4\pi\Delta^2 t^3}} \exp\left[-\frac{\Gamma(t-\Gamma)^2}{4\Delta^2 t}\right] \quad (\text{eq. 4})$$

where  $\Gamma$  is the mean age and  $\Delta$  is the width, or standard deviation, of the distribution (Wauugh et al., 2003).

Each water sample's measured CFC-11, CFC-12, and SF<sub>6</sub> were matched to a TTD lookup table (Stanley et al., 2012; Sonnerup et al., 2015) that allowed for  $\Delta/\Gamma$  to range, in 0.1 increments, from 0.3 up to 1.8, the range that can be constrained by those three tracers (Stöven et al., 2015), and included each TTD's atmospheric N<sub>2</sub>O, below. The matching criterion was within  $\pm 3\sigma$  of the combined tracer measurement and tracer saturation level uncertainties. The saturation levels dominate the uncertainty. Saturation levels of CFC-11, CFC-12, and SF<sub>6</sub> were estimated from the outcropping region of the respective isopycnals.

#### 2.4.1 N<sub>2</sub>O atmospheric history

The N<sub>2</sub>O atmospheric history post-1800 was estimated using the polynomial fit presented in Freing et al. (2009), updated to the present using annual global mean N<sub>2</sub>O atmospheric mixing ratios from the NOAA Earth System Research Laboratory (ESRL) Global Monitoring Division (<https://www.esrl.noaa.gov/gmd/hats/combined/N2O.html>). Pre-1800, a constant N<sub>2</sub>O mixing ratio of 274.81 ppb was used.

#### 2.4.2 Using TTDs to constrain biogenic N<sub>2</sub>O

The total N<sub>2</sub>O in a water parcel (N<sub>2</sub>O<sub>obs</sub>) is the sum of N<sub>2</sub>O from two different sources: 1) equilibrated from the atmosphere at the time it was last at the surface (N<sub>2</sub>O<sub>bkg</sub>) and 2) added from microbial processes ( $\Delta$ N<sub>2</sub>O or N<sub>2</sub>O<sub>prod</sub>):

$$\Delta\text{N}_2\text{O} = [\text{N}_2\text{O}]_{\text{prod}} = [\text{N}_2\text{O}]_{\text{obs}} - [\text{N}_2\text{O}]_{\text{bkg}} \quad (\text{eq. 5})$$

$$[\text{N}_2\text{O}]_{\text{bkg}} = X_{\text{N}_2\text{O}} \times P \times F_{\text{T,S}} \quad (\text{eq. 6})$$

where  $X_{\text{N}_2\text{O}}$  is the atmospheric mixing ratio of N<sub>2</sub>O,  $P$  is the atmospheric pressure, and  $F_{\text{T,S}}$  is the temperature and salinity dependent solubility of N<sub>2</sub>O in seawater (Weiss and Price, 1980). The N<sub>2</sub>O mixing ratio of the TTDs for each water parcel were calculated using the atmospheric history of N<sub>2</sub>O. The TTDs' N<sub>2</sub>O mixing ratio were used to calculate the N<sub>2</sub>O concentration at atmospheric equilibrium (N<sub>2</sub>O<sub>bkg</sub>) for each water sample. For values where the CFC-11 was below detection ( $< 0.001$  pmol kg<sup>-1</sup>), an atmospheric N<sub>2</sub>O mixing ratio of 274.81 ppb was used.

### 2.5 Keeling plot analysis

In order to determine the sources of high  $\Delta$ N<sub>2</sub>O near the oxycline in the ETNP and ETSP ODZs, the isotopic and

isotopomer compositions of the N<sub>2</sub>O produced within given water masses and at different O<sub>2</sub> concentrations were estimated using Keeling plot analysis (Keeling, 1961; Pataki et al., 2003; Yamagishi et al., 2007; Fujii et al., 2013; Casciotti et al., 2018). The isotopic composition of source N<sub>2</sub>O was determined using equation 5 and:

$$\delta_{\text{obs}} \times [\text{N}_2\text{O}]_{\text{obs}} = \delta_{\text{bkg}} \times [\text{N}_2\text{O}]_{\text{bkg}} + \delta_{\text{prod}} \times [\text{N}_2\text{O}]_{\text{prod}} \quad (\text{eq. 7})$$

where the obs, prod and bkg subscripts refer to N<sub>2</sub>O measured, newly produced and at equilibrium, respectively.

Rearranging equations 5 and 7 gives:

$$\delta_{\text{obs}} = 1/[\text{N}_2\text{O}]_{\text{obs}} \times (\delta_{\text{bkg}} - \delta_{\text{prod}} \times [\text{N}_2\text{O}]_{\text{bkg}} + \delta_{\text{prod}}) \quad (\text{eq. 8})$$

The intercepts of the linear regression between the inverse of measured N<sub>2</sub>O concentration and the  $\delta^{15}\text{N}^{\text{bulk}}$ ,  $\delta^{15}\text{N}^{\alpha}$ ,  $\delta^{15}\text{N}^{\beta}$ ,  $\delta^{18}\text{O}$  and SP thus represents the isotopic composition of produced N<sub>2</sub>O.

### 2.6 Isotope effects during N<sub>2</sub>O consumption

We estimated isotope effects associated with N<sub>2</sub>O consumption in the ETNP ODZ using a closed-system Rayleigh model (Mariotti et al., 1981). Only data in the ETNP ODZ at [O<sub>2</sub>]  $< 5$   $\mu\text{mol kg}^{-1}$  where N<sub>2</sub>O consumption occurs were selected for this analysis.

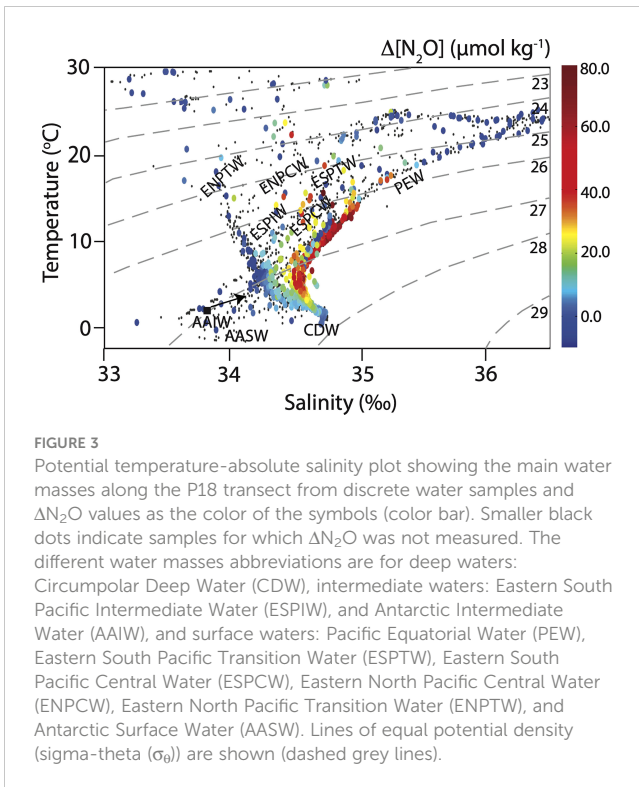
$$\delta\text{N}_2\text{O} = \delta\text{N}_2\text{O}_{\text{initial}} - \epsilon \ln([\text{N}_2\text{O}]_{\text{obs}}/[\text{N}_2\text{O}]_{\text{initial}}) \quad (\text{eq. 9})$$

where  $\delta^{15}\text{N}_2\text{O}$  is the  $\delta^{15}\text{N}^{\text{bulk}}$ ,  $\delta^{15}\text{N}^{\alpha}$ ,  $\delta^{15}\text{N}^{\beta}$ ,  $\delta^{18}\text{O}$  or SP for samples at O<sub>2</sub>  $< 5$   $\mu\text{mol kg}^{-1}$  (mostly in the ETNP ODZ), and the subscript refers to N<sub>2</sub>O measured and initial concentrations and isotopic values before the onset of N<sub>2</sub>O consumption. The isotope effects were estimated as the slopes of the linear regressions between  $\delta\text{N}_2\text{O}$  versus  $-\ln[\text{N}_2\text{O}]$ ,  $-\ln[\text{N}_2\text{O}]$  being an approximation of the  $[\text{N}_2\text{O}]_{\text{obs}}/[\text{N}_2\text{O}]_{\text{initial}}$  term.

## 3 Results

### 3.1 Water mass characterization

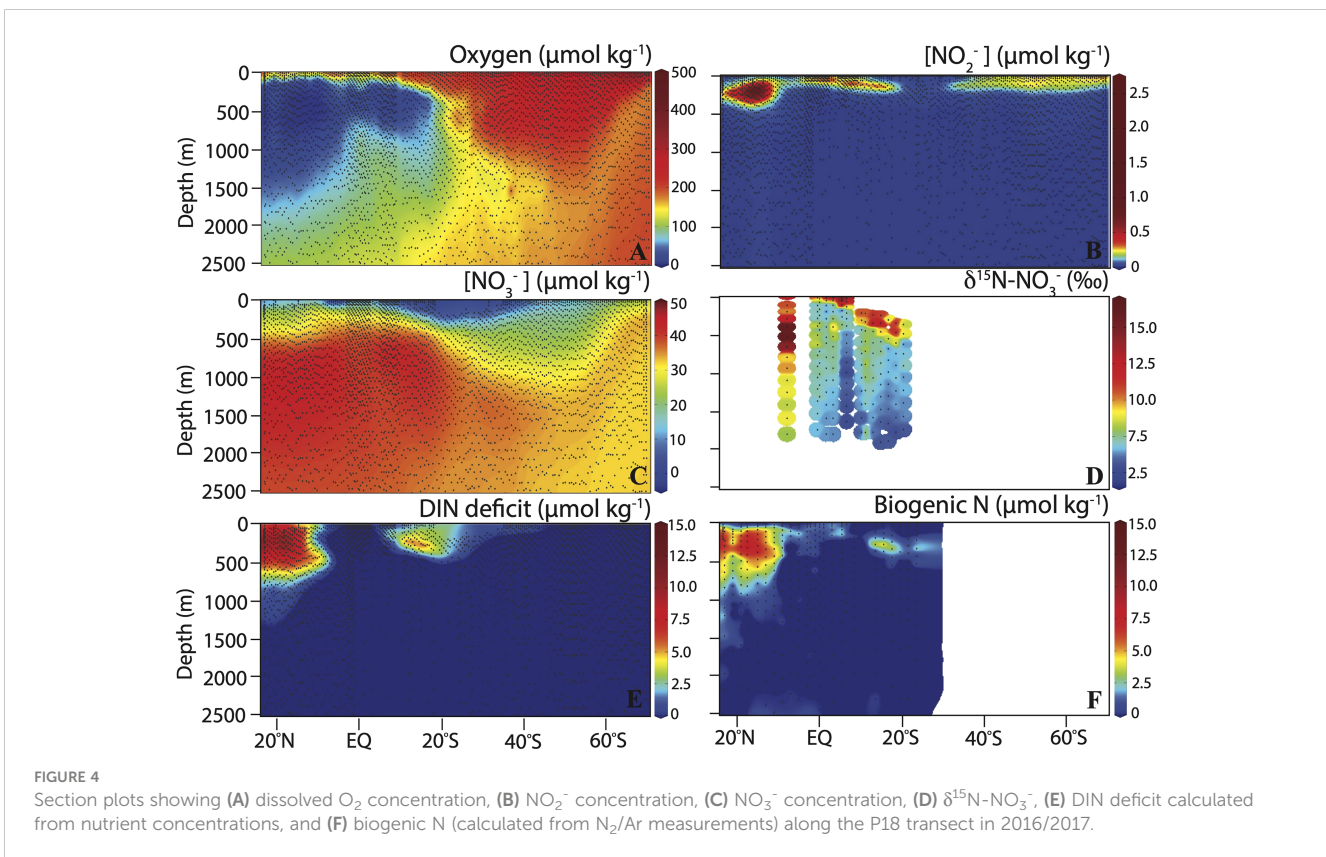
Water masses were characterized according to Emery (2001). The main surface water (0 – 500 m depth) masses along the P18 transects, listed from north to south with potential temperature and absolute salinity ranges in brackets, were Eastern North Pacific Central Water (ENPCW; 12.0–20°C; 34.2–35.0), Eastern North Pacific Transition Water (ENPTW; 11.0–20.0°C, 33.3–34.3), Pacific Equatorial Water (PEW; 7.0–23.0°C, 34.5–36.0), Eastern South Pacific Central Water (ESPCW; 8.0–24°C; 34.4–36.4), Eastern South Pacific Transition Water (ESPTW; 14.0–20.0°C; 34.6–35.2), and Antarctic Surface Water (AASW; -1.0–1.0°C, 34.0–34.6). Intermediate water masses (500 – 1500 m depth) include Eastern South Pacific Intermediate Water (ESPIW; 10.0–12.0°C, 34.0–34.3) and Antarctic Intermediate Water (2–10°C, 33.8–34.5). Circumpolar Deep Water (CDW; 0.1–2.0°C, 34.62–34.73) was observed below 1500 m depth (Figure 3).



### 3.2 Distribution of $\text{O}_2$ , nutrient concentrations, $\text{NO}_3^-$ isotopes, DIN deficit and biogenic N

The P18 transects crossed the ETNP ODZ and the fringe of the ETSP ODZ.  $\text{O}_2$  concentrations decreased to  $< 5 \mu\text{mol kg}^{-1}$  between 120 m and 845 m depth in the northernmost part of the transect in the ETNP ODZ. In the ETSP,  $\text{O}_2$  concentrations generally remained  $> 5 \mu\text{mol kg}^{-1}$ , except at few stations/depths between  $4.5^\circ\text{S}$  and  $9.7^\circ\text{S}$  and 195 and 495 m depth. The oxycline depth varied between 70 m at  $10.5^\circ\text{N}$  to 285 m at  $16^\circ\text{S}$  (Figure 4A).

Nitrite concentrations were generally low ( $< 2.7 \mu\text{mol kg}^{-1}$ ), with highest concentrations between  $13^\circ\text{N}$  and  $16^\circ\text{N}$  and 110 m to 285 m depth in the ETNP ODZ. Nitrite also accumulated at the fringe of the ETSP ODZ, with maximum concentrations between  $7.5^\circ\text{S}$  and  $16.5^\circ\text{S}$  near 100 m depth. Modest nitrite accumulations ( $< 0.5 \mu\text{mol kg}^{-1}$ ) were also observed in the upper 200 m from  $34^\circ\text{S}$  to  $60^\circ\text{S}$  (Figure 4B). Nitrate concentrations were generally depleted in surface waters, with the deepest maximum nitracline found at 350 m depth in the oligotrophic subtropical South Pacific from  $21^\circ\text{S}$  to  $31.5^\circ\text{S}$  (Figure 4C). A high  $\delta^{15}\text{N}$  of  $\text{NO}_3^-$  of up to  $\sim 15\text{‰}$  was observed in surface waters (Figure 4D), as expected following fractionation during  $\text{NO}_3^-$  assimilation by phytoplankton (Altabet, 2001; Granger et al., 2004). Nitrate concentrations were



moderate in the upper 500 m of the ETNP ODZ (minimum  $[\text{NO}_3^-]$  of  $21 \mu\text{mol kg}^{-1}$ , corresponding to ENPCW). The  $\delta^{15}\text{N}$  of  $\text{NO}_3^-$  was also elevated in the ODZ (up to 16.7‰ at 8.5°N and 425 m depth), consistent with fractionation during denitrification (Cline and Kaplan, 1975; Granger et al., 2008). Nitrate accumulation of up to  $45 \mu\text{mol kg}^{-1}$  were observed between 625 and 1750 m depth and was more pronounced in the ETNP. Nitrate concentrations remained relatively constant below 2000 m depth, with higher concentrations ( $\sim 38 \mu\text{mol kg}^{-1}$ ) in the northern portion of the transect compared to the South ( $\sim 33 \mu\text{mol kg}^{-1}$ ) (Figures 4C, D).

The DIN deficit (Howell et al., 1997) was calculated using the following equations:

$$\text{DIN deficit} = \text{DIN}_{\text{exp}} - \text{DIN}_{\text{obs}} \quad (\text{eq. 10})$$

$$\text{DIN}_{\text{exp}} = m \times [\text{PO}_4^{3-}]_{\text{obs}} + b \quad (\text{eq. 11})$$

where  $\text{DIN}_{\text{exp}}$  is the concentrations of dissolved inorganic nitrogen expected assuming Redfield stoichiometry (typically 16N:1P),  $\text{DIN}_{\text{obs}}$  is the concentration of nitrate plus nitrite measured and  $m$  and  $b$  are the slope and intercept, respectively, of the relationship between DIN and phosphate ( $\text{PO}_4^{3-}$ ) concentrations for source waters outside of the ETNP and ETSP ODZs.  $\text{DIN}_{\text{exp}}$  was calculated according to Chang et al. (2010; Chang et al., 2012). DIN deficit was particularly elevated (up to  $13.75 \mu\text{mol kg}^{-1}$ ) between 50 and 580 m depth in the ETNP ODZ. DIN deficit was also elevated at the fringes of the ETSP ODZ, with values of up to  $12.4 \mu\text{mol kg}^{-1}$  at 9.7°S and 205 m depth. Biogenic N

derived from  $\text{N}_2/\text{Ar}$  data (as  $\mu\text{mol N kg}^{-1}$ ) were generally comparable to DIN deficit, although generally a bit lower. Discrepancy between these two measurements could be caused by collection ( $\text{N}_2/\text{Ar}$  was not a prioritized gas sample during the P18 cruise) and/or storage effects for the  $\text{N}_2/\text{Ar}$  samples (Figures 4E, F).

### 3.3 $\Delta\text{N}_2\text{O}$ , $\text{N}_2\text{O}$ stable isotopes and isotopomers

The largest  $\Delta\text{N}_2\text{O}$  accumulation of  $75.7 \text{ nmol kg}^{-1}$  at  $[\text{O}_2] < 5 \mu\text{mol kg}^{-1}$  was observed at a depth of 95 m ( $\sigma_\theta = 25.65$ ), near the oxycline in the ENPCW water mass in the ETNP ODZ (14.5°N) (Figure 5A). High  $\Delta\text{N}_2\text{O}$  of up to  $73 \text{ nmol kg}^{-1}$  were also observed under low- $\text{O}_2$  conditions ( $15 \mu\text{mol kg}^{-1}$ ) at the fringe of the ETSP ODZ (7–9°S) at 180–195 m depth ( $\sigma_\theta = 26.4$ ), which corresponds to the PEW water mass (Figures 3, 5). Overall, elevated  $\Delta\text{N}_2\text{O}$  concentrations ( $>30 \text{ nmol kg}^{-1}$ ) were observed from the northern portion of the P18 transect to about 20°S, clearly associated with low- $\text{O}_2$  waters from the ETNP and ETSP ODZs. In contrast, slightly negative  $\Delta\text{N}_2\text{O}$  (undersaturation) ( $\sim -1 \text{ nmol kg}^{-1}$ ) values were observed in surface waters at the southern part of the transect associated with the subduction of AASW forming AAIW (Emery, 2001). Rapid cooling and sinking of surface water, with insufficient time for re-equilibration with the atmosphere, is likely causing the observed  $\text{N}_2\text{O}$  undersaturation in near surface waters in this region. A slight increase in  $\Delta\text{N}_2\text{O}$  (up to  $\sim 20 \text{ nmol kg}^{-1}$ ) was observed from

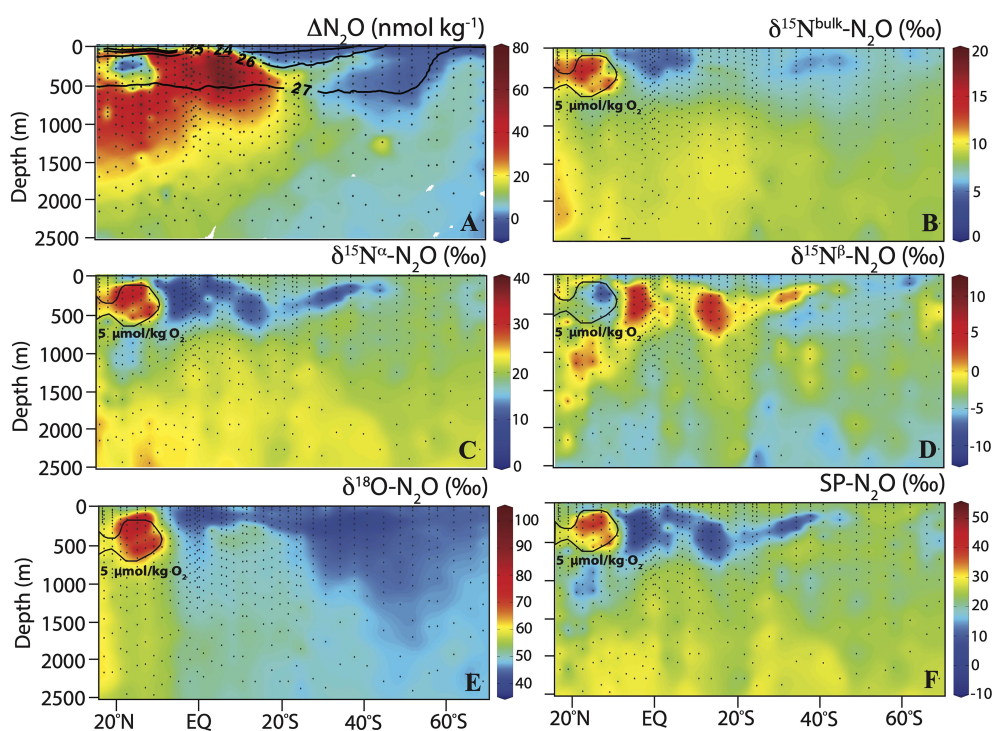


FIGURE 5

Section plots of (A)  $\Delta\text{N}_2\text{O}$  with sigma-theta ( $\sigma_\theta$ ;  $\text{kg m}^{-3}$ ) in overlay, (B)  $\delta^{15}\text{N}^{\text{bulk}}\text{-N}_2\text{O}$ , (C)  $\delta^{15}\text{N}^\alpha\text{-N}_2\text{O}$ , (D)  $\delta^{15}\text{N}^\beta\text{-N}_2\text{O}$ , (E)  $\delta^{18}\text{O}\text{-N}_2\text{O}$ , and (F)  $\text{SP}\text{-N}_2\text{O}$  along the P18 transect. The  $5 \mu\text{mol kg}^{-1} \text{O}_2$  contour in the ETNP is shown in (B–F).

60°S to 20°S in AAIW waters. Negative  $\Delta\text{N}_2\text{O}$  (minimum of  $\sim -5$   $\text{nmol kg}^{-1}$ ) were observed within the anoxic zone ( $\text{O}_2 < 5 \mu\text{mol kg}^{-1}$ ) of the ETNP (Figure 5A).

The  $\delta^{15}\text{N}^{\text{bulk}}\text{-N}_2\text{O}$  was lowest in the first 500 m depth near the equator, with values less than 5‰, indicating production (Figure 5B). The highest  $\delta^{15}\text{N}^{\text{bulk}}\text{-N}_2\text{O}$  values (up to 18‰) were observed within the ETNP ODZ, consistent with the observed low  $\Delta\text{N}_2\text{O}$  and indicating net consumption (Ostrom et al., 2007).  $\delta^{15}\text{N}^{\text{bulk}}\text{-N}_2\text{O}$  remained approximately 8 to 10‰ in waters deeper than 1000 m depth. The  $\delta^{15}\text{N}^{\alpha}\text{-N}_2\text{O}$  nearly followed the same distribution pattern as  $\delta^{15}\text{N}^{\text{bulk}}\text{-N}_2\text{O}$ , with overall higher values (up to 42.5‰) in the ETNP ODZ (Figure 5C). The  $\delta^{15}\text{N}^{\beta}\text{-N}_2\text{O}$  contrasted with the  $\delta^{15}\text{N}^{\text{bulk}}\text{-N}_2\text{O}$  and  $\delta^{15}\text{N}^{\alpha}\text{-N}_2\text{O}$  distributions, with highest values (up to 9.4‰) within the first 500 m flanking the equator and lowest values (minimum of -11.3‰) in the ETNP ODZ (Figure 5D). The  $\delta^{18}\text{O}\text{-N}_2\text{O}$  decreased along the north-south gradient of the P18 transect, with highest values (up to 100‰) in the ETNP ODZ (Figure 5E).  $\delta^{18}\text{O}\text{-N}_2\text{O}$  remained fairly constant below 2000 m depth and increased from  $\sim 48$  to 56‰ in CDW from south to north along the P18 transect. SP distribution was similar to that of  $\delta^{15}\text{N}^{\alpha}\text{-N}_2\text{O}$ , with lowest values (minimum of -6.1‰) in low  $\text{O}_2$  waters ( $>5 \mu\text{mol kg}^{-1}$ ) in the upper 500 m near the equator and highest values (up to 49‰) in the ETNP ODZ (Figure 5F). In AASW and AAIW at the southern portion of the transect near Antarctica,  $\delta^{15}\text{N}^{\text{bulk}}$ ,  $\delta^{15}\text{N}^{\alpha}$ ,  $\delta^{15}\text{N}^{\beta}$ ,  $\delta^{18}\text{O}$  and SP were close to

atmospheric  $\text{N}_2\text{O}$  values (6.2‰ for  $\delta^{15}\text{N}^{\text{bulk}}$ , 15.8‰ for  $\delta^{15}\text{N}^{\alpha}$ , -3.4‰ for  $\delta^{15}\text{N}^{\beta}$ , 44.3‰ for  $\delta^{18}\text{O}$  and 19.2‰ for SP; Kelly et al., 2021). The isotopic signatures of  $\text{N}_2\text{O}$ , together with the observed slight  $\text{N}_2\text{O}$  undersaturation, indicate no  $\text{N}_2\text{O}$  production in this region.

### 3.4 Relationships between $\Delta\text{N}_2\text{O}$ , AOU and N deficit

The ratio between  $\Delta\text{N}_2\text{O}/\text{AOU}$ , indicative of cumulative  $\text{N}_2\text{O}$  production yield, increased at low  $\text{O}_2$  concentration to 0.3 (Figure 6A). Other high  $\Delta\text{N}_2\text{O}/\text{AOU}$  ratios observed at higher  $\text{O}_2$  concentrations were clearly influenced by the contrasting effect of photosynthesis on AOU, as indicated by higher pH at these shallower isopycnal ranges (Supplementary materials, Figure S1). The lowest SPs were observed at highest  $\Delta\text{N}_2\text{O}$  and  $\Delta\text{N}_2\text{O}/\text{AOU}$  ratios (Figure 6B). Positive relationships between  $\Delta\text{N}_2\text{O}$  and AOU were observed in surface waters  $\sigma_{\theta} < 26 \text{ kg m}^{-3}$  in the ETNP and ETSP (Supplementary materials, Figure S2). No significant relationship between  $\Delta\text{N}_2\text{O}$  and AOU was observed at  $26 < \sigma_{\theta} < 27 \text{ kg m}^{-3}$  where highest  $\Delta\text{N}_2\text{O}$  values were generally observed.

Significant positive relationships between  $\Delta\text{N}_2\text{O}$  and DIN deficit were observed in the ETNP (18.5°N – Equator), with an increased slope toward deeper isopycnals where highest  $\Delta\text{N}_2\text{O}$  were

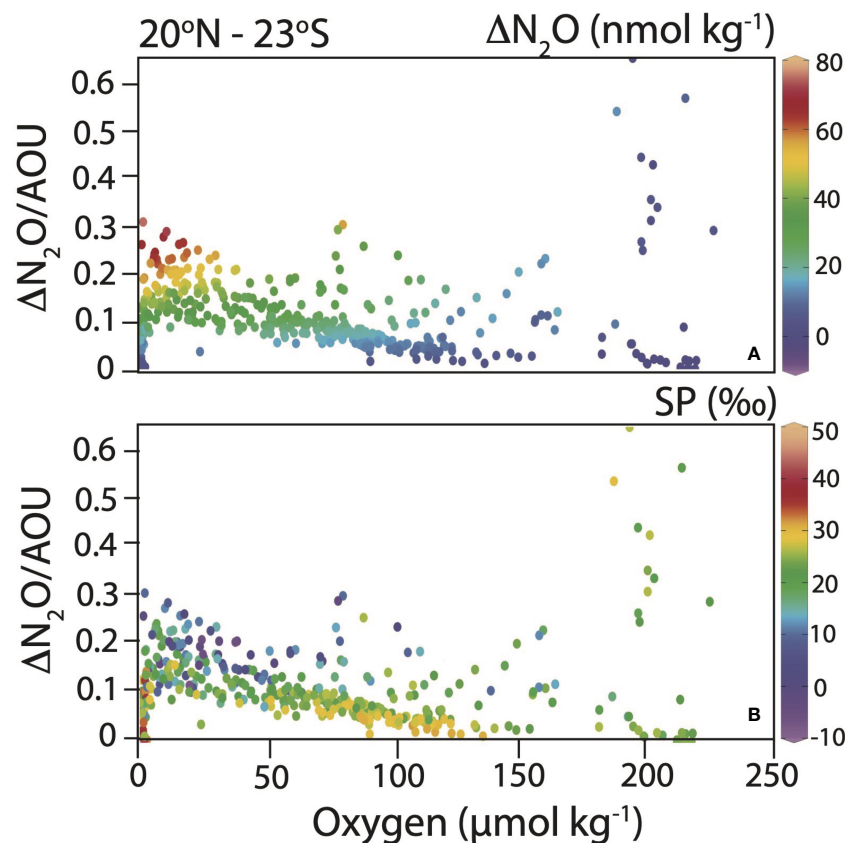
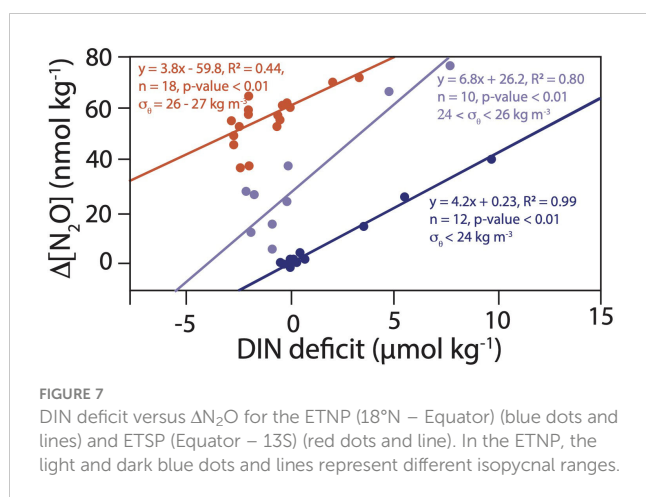


FIGURE 6

$\Delta\text{N}_2\text{O}/\text{AOU}$  versus  $\text{O}_2$  concentration showing increased  $\text{N}_2\text{O}$  production yield (associated with low SP) under low  $\text{O}_2$  conditions.  $\Delta\text{N}_2\text{O}$  (A) and SP (B) are shown as the color of the symbols (see color bars).



observed. A significant positive relationship between  $\Delta N_2O$  and DIN deficit was also observed in the ETSP (Equator – 13°S) for the isopycnal range  $26 < \sigma_\theta < 27 \text{ kg m}^{-3}$ . No such relationship was observed in the ETSP surface waters ( $\sigma_\theta < 26 \text{ kg m}^{-3}$ ) (Figure 7).

## 4 Discussion

### 4.1 Sources of the highest $\Delta N_2O$ accumulations near the oxycline in the ETNP and ETSP

We observed relatively high  $N_2O$  concentrations of up to  $84 \text{ nmol kg}^{-1}$  (940% supersaturation) near the upper oxycline in offshore waters along the P18 section crossing the ETNP ODZ and the fringe of the ETSP ODZ. High  $N_2O$  concentrations of up to  $\sim 100 \text{ nmol kg}^{-1}$  were also observed offshore near the oxycline in the ETNP ODZ (Trimmer et al., 2016; Kelly et al., 2021). At offshore stations in the ETSP ODZ, Casciotti et al. (2018) observed  $N_2O$  concentrations were up to  $\sim 70 \text{ nmol kg}^{-1}$ , comparable to observations along the P18 line. In contrast, Bourbonnais et al. (2017) observed much higher  $N_2O$  concentrations of up to  $\sim 190 \text{ nmol kg}^{-1}$  in coastal surface waters off Peru in the ETSP ODZ. Differences in  $N_2O$  accumulation observed between these different studies appear to mostly relate to productivity (e.g., coastal versus offshore), but there is also evidence for dynamic  $N_2O$  cycling at offshore stations. For instance, the El Niño-Southern Oscillation and mesoscale processes such as eddies have been shown to influence  $N_2O$  distribution (e.g., Arévalo-Martínez et al., 2016; Ji et al., 2019; Babbín et al., 2020; Monreal et al., 2022).

Yield of  $N_2O$  from nitrification increased toward lower  $[O_2]$ , as also observed in previous studies (e.g., Ryabenko et al., 2012; Ji et al., 2015; Ji et al., 2018; Frey et al., 2020) (Figure 6). If we assume that 138 moles of  $O_2$  are reduced for 16 moles of  $NH_4^+$  nitrified (Ward, 2008), a yield of up to 0.5%  $N-N_2O$  mol produced per mol  $NH_4^+$  oxidized is obtained considering the highest  $\Delta N_2O/AOU$  slope of 0.3. A 0.5% yield falls in the range observed in the Pacific Ocean (Yoshida et al., 1989), but is lower than the maximum  $N_2O$  production yield for nitrification reported for  $^{15}N$ -labeled incubation studies (up to  $\sim 3\%$  in the ETSP ODZ) (Ji et al., 2018;

Frey et al., 2020). However, while nitrification is clearly occurring in surface waters along the P18 transect, as shown by correlations between  $\Delta N_2O$  and AOU, the data deviate from this relationship on isopycnals where the highest  $\Delta N_2O$  were observed near the ODZ oxycline (Supplementary materials, Figure S2).

Two different sources of  $N_2O$  were observed from the Keeling plot analysis in both the ETNP and ETSP for  $[O_2] > 5 \text{ } \mu\text{mol kg}^{-1}$  and  $\sigma_\theta < 27 \text{ kg m}^{-3}$  (Figures 8, 9). A break-point analysis was performed in R using the package “segmented” (Muggeo, 2003; Muggeo and Muggeo, 2017) as described in Kelly et al. (2021). The breakpoint was around  $33 \text{ nmol kg}^{-1}$  ( $1/[N_2O] = 0.03$ ) in both regions. Coincidentally, this analysis divided the data into two main  $O_2$  regimes:  $5 \text{ } \mu\text{mol kg}^{-1} < [O_2] < 100 \text{ } \mu\text{mol kg}^{-1}$  and  $[O_2] > 100 \text{ } \mu\text{mol kg}^{-1}$  (Table 1). It should be noted that highest  $\Delta N_2O$  in the ETNP were observed at  $[O_2]$  below  $5 \text{ } \mu\text{mol kg}^{-1}$  and were thus not included in the Keeling plot analysis. Kelly et al. (2021) found a clear relationship between distinct  $N_2O$  sources and  $[NO_2^-]$ , with highest  $N_2O$  accumulation at elevated  $[NO_2^-]$  (up to  $\sim 1 \text{ } \mu\text{mol kg}^{-1}$ ) in the ETNP. In contrast to Kelly et al. (2021), no such relationship was observed when restricting the dataset to the same isopycnal range ( $\sigma_\theta \leq 25 \text{ kg m}^{-3}$ ).

The  $\delta^{15}N^{\text{bulk}}$  of source  $N_2O$  varied from 4.0 to 7.2‰ (Table 1).  $\delta^{15}N^{\text{bulk}}$  is affected by the  $\delta^{15}N$  of the substrate and fractionation effects during  $N_2O$  production (e.g., Sutka et al., 2006; Frame et al., 2014; Bourbonnais et al., 2017). Similar  $\delta^{15}N^{\text{bulk}}$  values for source  $N_2O$  were reported in the ETSP (Casciotti et al., 2018). These values fall within the expected range for the  $\delta^{15}N$  of remineralized  $NH_4^+$ , the substrate for nitrification, assuming a  $\delta^{15}N$  of sinking particulate matter of 3–15‰ (Altabet et al., 1999; Altabet, 2001; Berelson et al., 2015) in the eastern Pacific and a modest isotope effect during ammonification (Altabet, 1988).  $N_2O$  could also be produced by denitrification as the  $\delta^{15}N$  of  $NO_3^-$  observed in this study (4.5–15.4‰) was also similar to observed  $\delta^{15}N^{\text{bulk}}-N_2O$  values. However, the upper range in  $\delta^{15}N$  values for these substrates is needed to reproduce the observed  $\delta^{15}N^{\text{bulk}}-N_2O$  during nitrification and denitrification as both processes are expected to add a lower  $\delta^{15}N$  due to isotopic fractionation, unless the substrate is completely consumed, or the reaction is diffusion limited (see Table 1 in Bourbonnais et al., 2017 for a compilation of  $\epsilon$  associated with these processes and Ostrom and Ostrom, 2012; Frame et al., 2014).

A high  $\delta^{18}O$  (52.3‰) and relatively low  $\delta^{15}N^\alpha$  (2.7‰) and SP (-9.0‰) were estimated for source  $N_2O$  in the ETNP just above the ODZ corresponding to highest  $\Delta N_2O$  accumulations. In contrast,  $\delta^{15}N^{\text{bulk}}$ ,  $\delta^{15}N^\alpha$ ,  $\delta^{15}N^\beta$ ,  $\delta^{18}O$  and SP of source  $N_2O$  in surface waters ( $[O_2]$  higher than  $100 \text{ } \mu\text{mol kg}^{-1}$ ) were more comparable to atmospheric signatures (Table 1). In the ETSP, the  $\delta^{15}N^\alpha$  (11.0‰),  $\delta^{18}O$  (55.7‰) and SP (9.5‰) of source  $N_2O$  were higher than in the ETNP near the oxycline and the SP in oxic surface waters (11.3‰) was significantly lower. The isotopic values of source  $N_2O$  observed in surface waters overlying the ODZ in the ETSP contrasted with the values estimated by Casciotti et al. (2018). For instance, the  $\delta^{18}O$  was significantly lower and the SP was higher than the values reported by Casciotti et al. (2018) (Table 1). These differences were likely caused by spatial and/or temporal heterogeneity. Moreover, P18 only crossed the fringe of the ETSP ODZ, with  $[O_2]$  generally higher than  $5 \text{ } \mu\text{mol kg}^{-1}$ , except at a few stations/depths.

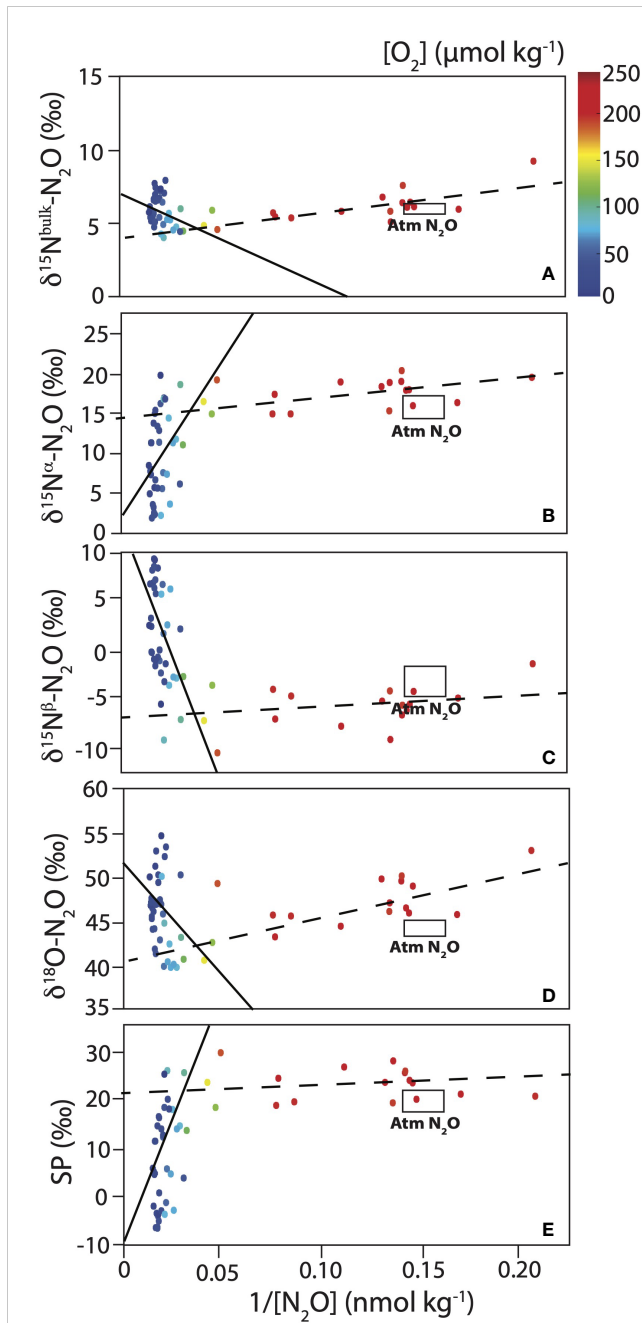


**FIGURE 8**  
Keeling plot analysis for the ETNP (18°N – Equator) for (A)  $\delta^{15}\text{N}^{\text{bulk}}$ , (B)  $\delta^{15}\text{N}^{\alpha}$ , (C)  $\delta^{15}\text{N}^{\beta}$ , (D)  $\delta^{18}\text{O}$  and (E) SP of  $\text{N}_2\text{O}$  (in ‰). Black lines are linear regressions (full line:  $5 \mu\text{mol kg}^{-1} < [\text{O}_2] < 100 \mu\text{mol kg}^{-1}$  and dashed line:  $[\text{O}_2] > 100 \mu\text{mol kg}^{-1}$ ).  $\text{O}_2$  concentrations are shown as the color of the symbols (see color bar in top panel). Atmosphere  $\text{N}_2\text{O}$  isotopic values are shown as a rectangle (from Kelly et al., 2021). See Table 1 for intercept,  $R^2$  and p-value for the linear regressions.

The stable isotopic and isotopomer signatures observed at the highest  $\Delta\text{N}_2\text{O}$  and lowest  $[\text{O}_2]$  near the oxycline in both the ETNP and ETSP are consistent with production from denitrification or nitrifier-denitrification. SP is particularly useful for differentiating  $\text{N}_2\text{O}$  production processes as it is mainly pathway dependent and independent of the isotopic composition of the substrate (Schmidt et al., 2004; Sutka et al., 2004). For instance, formation of  $\text{N}_2\text{O}$

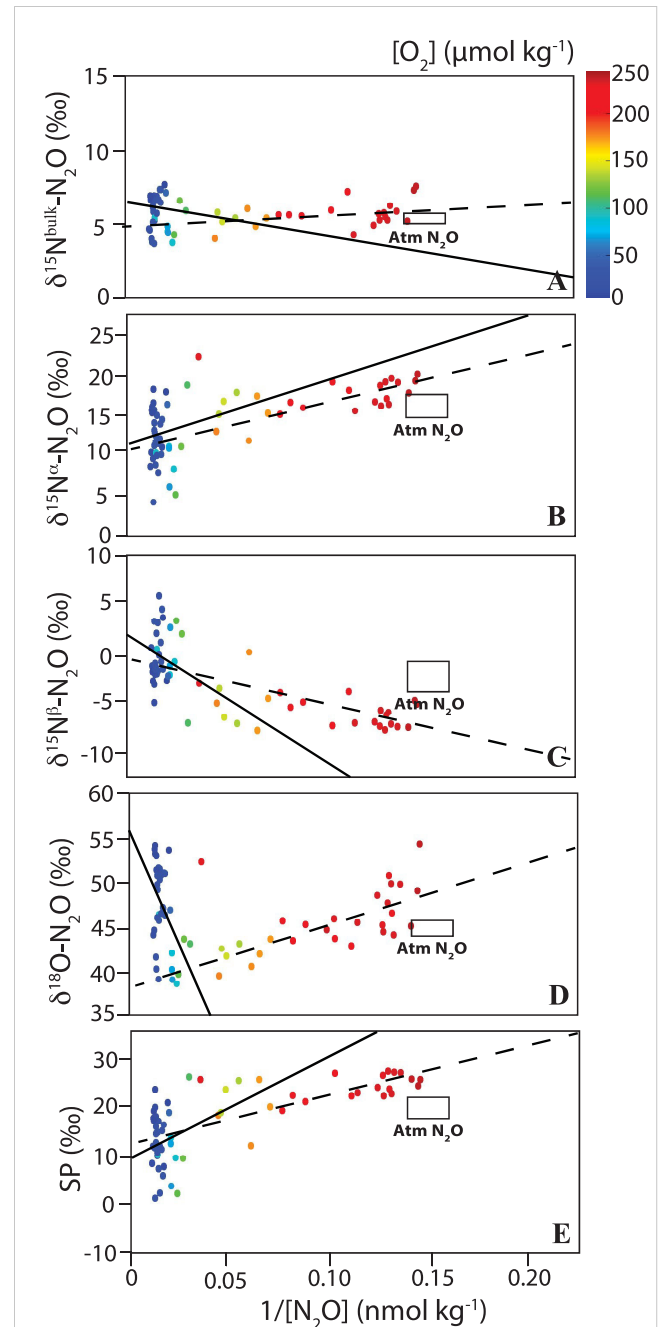


**FIGURE 9**  
Keeling plot analysis for the ETSP (Equator – 13°S) for (A)  $\delta^{15}\text{N}^{\text{bulk}}$ , (B)  $\delta^{15}\text{N}^{\alpha}$ , (C)  $\delta^{15}\text{N}^{\beta}$ , (D)  $\delta^{18}\text{O}$  and (E) SP of  $\text{N}_2\text{O}$  (in ‰). Black lines are linear regressions (full line:  $5 \mu\text{mol kg}^{-1} < [\text{O}_2] < 100 \mu\text{mol kg}^{-1}$  and dashed line:  $[\text{O}_2] > 100 \mu\text{mol kg}^{-1}$ ).  $\text{O}_2$  concentrations are shown as the color of the symbols (see color bar in top panel). Atmosphere  $\text{N}_2\text{O}$  isotopic values are shown as a rectangle (from Kelly et al., 2021). See Table 1 for intercept,  $R^2$  and p-value for the linear regressions.

during bacterial denitrification occurs by combining two NO molecules following a *trans* mechanism (Toyoda et al., 2005; Magyar, 2017). This mechanism involves the asymmetrical intermediate *trans*-hyponitrite ( $-\text{ONNO}-$ ) bridging two iron centers; the  $\alpha$  N atom and the O comes from NO bonded to  $\text{Fe}_{\text{heme}}$  and the  $\beta$  N atom comes from NO bonded to  $\text{Fe}_{\text{B}}$ . If the precursor NO molecules are derived from the same substrate, this

TABLE 1 Intercept (in ‰), R<sup>2</sup>, and p-values of linear regressions for Keeling plot analysis under different O<sub>2</sub> regimes and regions/water masses along the P18 line.

	$\delta^{15}\text{N}^{\text{bulk}}\text{-N}_2\text{O}$	$\delta^{15}\text{N}^{\alpha}\text{-N}_2\text{O}$	$\delta^{15}\text{N}^{\beta}\text{-N}_2\text{O}$	$\delta^{18}\text{O}\text{-N}_2\text{O}$	SP
<b>ETNP (18.5°N – EQ)</b>					
100 $\mu\text{mol kg}^{-1} > [\text{O}_2] > 5 \mu\text{mol kg}^{-1}$ ( $27 > \sigma_{\theta} > 23.3 \text{ kg m}^{-3}$ ) (n = 37)					
Intercept	7.2 ± 0.8	2.7 ± 4.0	11.7 ± 3.5	52.3 ± 3.2	-9.0 ± 7.3
R <sup>2</sup>	0.079	0.086	0.19	0.10	0.14
p-value	0.09	0.08	<0.01	0.06	0.02
[O <sub>2</sub> ] > 100 $\mu\text{mol kg}^{-1}$ (surface, $\sigma_{\theta} < 25.7 \text{ kg m}^{-3}$ ) (n = 18)					
Intercept	4.0 ± 0.4	12.3 ± 14.7	-6.5 ± 1.4	40.8 ± 1.4	20.7 ± 2.5
R <sup>2</sup>	0.59	0.038	0.045	0.54	0.06
p-value	<0.01	0.4	0.4	<0.01	0.3
Deep waters, $\sigma_{\theta} > 27.3 \text{ kg m}^{-3}$ (n = 47)					
Intercept	9.1 ± 5.0	16.8 ± 1.1	1.4 ± 0.9	52.7 ± 1.7	15.4 ± 2.0
R <sup>2</sup>	0.01	0.39	0.46	0.020	0.45
p-value	0.6	<0.01	<0.01	0.4	<0.01
<b>ETSP (13°S – EQ)</b>					
100 $\mu\text{mol kg}^{-1} > [\text{O}_2] > 5 \mu\text{mol kg}^{-1}$ ( $27 > \sigma_{\theta} > 26 \text{ kg m}^{-3}$ ) (n = 34)					
Intercept	6.3 ± 0.9	11.0 ± 2.6	1.6 ± 2.0	55.7 ± 3.3	9.5 ± 4.3
R <sup>2</sup>	0.0056	0.0084	0.035	0.17	0.020
p-value	0.7	0.6	0.3	0.01	0.4
[O <sub>2</sub> ] > 100 $\mu\text{mol kg}^{-1}$ (surface waters, $\sigma_{\theta} < 26 \text{ kg m}^{-3}$ ) (n = 26)					
Intercept	4.9 ± 0.4	10.6 ± 1.2	-0.7 ± 1.2	38.3 ± 1.2	11.3 ± 2.2
R <sup>2</sup>	0.12	0.54	0.37	0.59	0.49
p-value	0.08	<0.01	<0.01	<0.01	<0.01
Deep waters, $\sigma_{\theta} > 27 \text{ kg m}^{-3}$ (n = 26)					
Intercept	7.0 ± 0.2	17.0 ± 0.9	-3.0 ± 1.0	45.5 ± 0.7	20.0 ± 1.8
R <sup>2</sup>	0.67	0.34	0.0068	0.41	0.14
p-value	<0.01	<0.01	0.5	<0.01	<0.01
<b>AAIW</b>					
Intercept	9.4 ± 0.3	18.1 ± 0.8	0.8 ± 0.6	52.5 ± 0.6	17.2 ± 1.4
R <sup>2</sup>	0.42	0.020	0.42	0.67	0.19
p-value	<0.01	0.2	<0.01	<0.01	<0.01
<b>Casciotti et al. (2018) - ETSP</b>					
Surface	6.1 ± 1.4	na	na	53.0 ± 3.1	5.4 ± 4.4
Oxycline	7.5 ± 2.2	na	na	50.7 ± 3.6	9.3 ± 2.4
Deep	6.6 ± 0.6	na	na	54.3 ± 0.6	20.1 ± 0.5
<b>Kelly et al. (2021) – ETNP</b>					
Surface	na	6.6 ± 0.5	0.6 ± 0.5	46.3 ± 0.5	6.6 ± 2.3
Oxycline	na	2.9 ± 1.4	-3.8 ± 0.9	53.1 ± 1.3	5.9 ± 0.8

(Continued)

TABLE 1 Continued

	$\delta^{15}\text{N}^{\text{bulk}}\text{-N}_2\text{O}$	$\delta^{15}\text{N}^{\alpha}\text{-N}_2\text{O}$	$\delta^{15}\text{N}^{\beta}\text{-N}_2\text{O}$	$\delta^{18}\text{O}\text{-N}_2\text{O}$	SP
Deep	6.2 ± 1.0	16.8 ± 0.	-4.5 ± 0.6	57.3 ± 0.8	21.3 ± 1.0
Atmosphere-equilibrated seawater (Kelly et al., 2021)	6.2 ± 0.4	15.8 ± 1.4	-3.4 ± 1.6	44.3 ± 0.8	19.2 ± 2.9

Standard error of the intercept is reported. P-value associated with a confidence level >90% are in bold. Atmospheric values are from Kelly et al. (2021). na means non available. AAIW temperature and salinity ranges are defined as in Emery (2001) (section 3.1).

mechanism causes little difference between the  $\delta^{15}\text{N}$  of the  $\alpha$  and  $\beta$  N atoms, resulting in a low SP (see Magyar, 2017 for more detail). In contrast, during  $\text{N}_2\text{O}$  formation according to a *cis* mechanism, a first NO molecule binds to one or the other iron center with the second NO molecule binding directly to the first NO, forming a symmetrical intermediate. Cleavage of  $^{14}\text{N}\text{-O}$  bond is preferred over  $^{15}\text{N}\text{-O}$  bond, leading to enrichment of the  $\alpha$  position and a higher SP. Thus,  $\text{N}_2\text{O}$  produced by nitrification, either by archaea and bacteria, is generally associated with a high SP of 30–38‰ consistent with a *cis*-formation mechanism (Sutka et al., 2003; Sutka et al., 2004; Frame and Casciotti, 2010; Santoro et al., 2011; Löscher et al., 2012) whereas denitrification and nitrifier-nitrification are associated with much lower SPs ( $\sim -10$  to 0‰) (Sutka et al., 2003; Sutka et al., 2004; Toyoda et al., 2005; Frame and Casciotti, 2010).

$\text{N}_2\text{O}$  produced by denitrification is associated with a low SP of  $\sim -5$  to 0‰ and adds a relatively low  $\delta^{15}\text{N}$  (especially at the  $\alpha$  position) with an isotope effect ( $^{15}\epsilon$ ) ranging from 13–37‰ (Barford et al., 1999; Sutka et al., 2003; Sutka et al., 2004; Toyoda et al., 2005; Sutka et al., 2006; Frame and Casciotti, 2010). On the other hand, branching fractionation, i.e., the preferential loss of  $^{16}\text{O}$  relative to  $^{18}\text{O}$  during  $\text{NO}_3^-$  reduction to  $\text{N}_2\text{O}$ , is expected to lead to high  $\delta^{18}\text{O}\text{-N}_2\text{O}$  values (Casciotti et al., 2002; Frame et al., 2014). The  $\delta^{18}\text{O}\text{-N}_2\text{O}$  is affected by both the branching isotope effects ( $^{18}\epsilon$ ) of 25–30‰ for  $\text{NO}_3^-$  reduction to  $\text{NO}_2^-$  and 10–12‰ during  $\text{NO}_2^-$  reduction to  $\text{N}_2\text{O}$  during denitrification as well as the equilibration of  $\text{NO}_2^-$  O isotope with water (Casciotti et al., 2007; Casciotti and Buchwald, 2012). Nitrifier-denitrification is associated with a SP of -10–0‰ and adds a lower  $\delta^{15}\text{N}$  compared to denitrification due to a larger  $^{15}\epsilon$  ranging from 31–58‰. Furthermore, an effective O isotope effect ( $^{18}\epsilon$ ) of 8–12‰ was reported for  $\text{NO}_2^-$  reduction to  $\text{N}_2\text{O}$  during nitrifier denitrification (Sutka et al., 2003; Sutka et al., 2004; Sutka et al., 2006; Frame and Casciotti, 2010). Newly produced  $\delta^{18}\text{O}\text{-N}_2\text{O}$  values during nitrification and nitrifier denitrification are thus generally lower (13–35‰; Snider et al., 2012). Accordingly, low source  $\delta^{18}\text{O}\text{-N}_2\text{O}$  values were observed at  $[\text{O}_2] > 100 \mu\text{mol kg}^{-1}$  in the ETNP and ETSP whereas higher values were observed at deeper isopycnal ranges overlying the ODZs (Table 1), consistent with the dominance of  $\text{N}_2\text{O}$  production by nitrification in surface waters and denitrification at lower  $\text{O}_2$  concentrations near the oxycline.

Kelly et al. (2021) similarly observed two distinctive sources of  $\text{N}_2\text{O}$  in the ETNP above the  $\sigma_\theta < 25 \text{ kg m}^{-3}$  isopycnal. SPs of 6–8‰ were observed. Based on an isotopic mass balance and assuming that the SPs for  $\text{N}_2\text{O}$  produced during nitrification and denitrification are 30–38‰ and 0‰, respectively (Sutka et al., 2003; Sutka et al., 2004; Toyoda et al., 2005; Frame and Casciotti, 2010; Santoro et al., 2011; Löscher et al., 2012), about 80% of the

$\text{N}_2\text{O}$  production was attributed to denitrification or nitrifier-denitrification. Bourbonnais et al. (2017) and Casciotti et al. (2018) also observed low SPs (-3 to 10‰) corresponding to large  $\Delta\text{N}_2\text{O}$  accumulation near the oxycline above the ETSP ODZ. The much lower SP observed in the ETNP in this study (-9‰) preclude any contribution from nitrification. The higher SP (9.5‰) for source  $\text{N}_2\text{O}$  observed at low  $[\text{O}_2]$  near the fringe of the ETSP ODZ suggests a relatively minor contribution from nitrification ( $\sim 1/3$ ) and is consistent with the value reported by Casciotti et al. (2018). However, hybrid  $\text{N}_2\text{O}$  formation by archaea, where one atom is derived from nitric oxide (NO; from  $\text{NO}_2^-$ ) and the other from hydroxylamine ( $\text{NH}_2\text{OH}$ ; from  $\text{NH}_4^+$ ) was shown to be an important production pathway in marine environments and could possibly contribute to endmember signatures estimated from the Keeling plot analysis (Stieglmeier et al., 2014; Kozłowski et al., 2016; Trimmer et al., 2016; Frame et al., 2017). Frey et al. (2020) showed that hybrid  $\text{N}_2\text{O}$  production accounts for 70–85% of the total  $\text{N}_2\text{O}$  production from  $\text{NH}_4^+$  oxidation using  $^{15}\text{N}$ -labeled incubation experiments in the ETSP. SP may, in part, reflect the relative  $\delta^{15}\text{N}$  of the substrates for the  $\alpha$  and  $\beta$  positions during hybrid archaeal  $\text{N}_2\text{O}$  production rather than being indicative of a particular pathway (Casciotti et al., 2018). Therefore, if lower SP could be produced by archaeal hybrid  $\text{N}_2\text{O}$  production, the fraction of denitrification needed to explain low SP signatures associated with high  $\text{N}_2\text{O}$  supersaturations observed above or in the ODZs in this and previous studies would further decrease (Bourbonnais et al., 2017; Casciotti et al., 2018; Kelly et al., 2021).

The observed relationships between  $\Delta\text{N}_2\text{O}$  and DIN deficit at isopycnals  $\sigma_\theta < 26 \text{ kg m}^{-3}$  and the absence of clear relationships between  $\Delta\text{N}_2\text{O}$  and  $[\text{NO}_2^-]$  further support a role for denitrification (rather than nitrifier-denitrification) as the dominant  $\text{N}_2\text{O}$  production pathway in both the ETSP and the ETNP. The decreased slope for the  $\Delta\text{N}_2\text{O}$  versus DIN deficit relationship toward surface isopycnal ranges observed in the ETNP suggests decreased  $\text{N}_2\text{O}$  yield at higher  $[\text{O}_2]$  concentrations or mixing/dilution of  $\text{N}_2\text{O}$  produced by denitrification advected from below, especially for upwelling waters near the equator. The  $\delta^{15}\text{N}$  of  $\text{NO}_3^-$  provides more insights into  $\text{N}_2\text{O}$  sources yet these measurements were mostly available at ETSP stations. A plot of SP versus  $\Delta^{15}\text{N}$  ( $\delta^{15}\text{N}\text{-NO}_3^- - \delta^{15}\text{N}\text{-N}_2\text{O}$ ) showed that some of the highest  $\Delta\text{N}_2\text{O}$  datapoint indeed fell within the expected compositional fields for  $\text{N}_2\text{O}$  production by bacterial denitrification ( $\Delta\delta^{15}\text{N} = 0\text{--}35\%$ , SP:  $-5\text{--}0\%$ ) (Wankel et al. (2017) and references therein, Supplementary Figure S3). Some high  $\Delta\text{N}_2\text{O}$  were associated with relatively high SPs ( $> 10\%$ ), showing the overprinting effect of  $\text{N}_2\text{O}$  consumption during denitrification (Ostrom et al., 2007). Compositional field analysis (Figure S3) also suggests production by either archaeal and bacterial ammonia oxidation at higher  $[\text{O}_2]$

and lower  $\Delta N_2O$ . Bourbonnais et al. (2017) also invoked incomplete denitrification as a major pathway for extreme  $N_2O$  accumulation in newly upwelled surface waters off Peru based on the absence of a relationship between  $\Delta N_2O$  and apparent  $O_2$  utilization and significant relationships between  $NO_3^-$  and  $N_2O$  isotopes. The dominance of denitrification for  $N_2O$  production near the oxycline is also supported by  $^{15}N$ -tracer incubation studies in the ETSP ODZ.  $N_2O$  production rates were indeed one order of magnitude higher for denitrification compared to ammonia oxidation under low- $O_2$  conditions at the  $\Delta N_2O$  maximum just above the ETSP ODZ (Ji et al., 2015; Frey et al., 2020).

## 4.2 Sources of $N_2O$ below the ETNP and ETSP ODZs and in AAIW

$N_2O$  sources in deep ETNP and ETSP were also investigated using Keeling plot analysis (Supplementary materials, Figure S4 and Table 1). A deeper isopycnal range ( $\sigma_\theta > 27.3 \text{ kg m}^{-3}$ ) was selected for the ETNP due to the deeper ODZ at this location as in a previous study (Kelly et al., 2021). An isopycnal range with  $\sigma_\theta > 27 \text{ kg m}^{-3}$  was selected for the ETSP comparable to the  $\sigma_\theta$  range in Casciotti et al. (2018).  $N_2O$  source values of 9.1‰ ( $\delta^{15}N^{\text{bulk}}$ ), 16.8‰ ( $\delta^{15}N^\alpha$ ), 1.4‰ ( $\delta^{15}N^\beta$ ), 52.7‰ ( $\delta^{18}O$ ) and 15.4‰ (SP) were estimated below the ETNP ODZ (Table 1). In the ETSP, the Keeling plot analysis revealed values of 7.0‰ ( $\delta^{15}N^{\text{bulk}}$ ), 17.0‰ ( $\delta^{15}N^\alpha$ ), -3.0‰ ( $\delta^{15}N^\beta$ ), 45.5‰ ( $\delta^{18}O$ ) and 20.0‰ (SP). The generally higher  $\delta^{15}N^\beta$  as well as lower  $\delta^{18}O$  and SP compared to prior studies (Casciotti et al., 2018; Kelly et al., 2021) might be the result of a lesser influence from  $N_2O$  production and consumption in the ODZ since our analysis also included equatorial waters. Overall, these isotopic signatures suggest the dominance of  $N_2O$  production by nitrification in deeper waters below the ETNP and ESTP ODZs. In fact, our results are more in line with a  $N_2O$  source from nitrification as a relatively low  $\delta^{18}O$  is expected for this process (i.e., 13–35‰; Snider et al., 2012).

The sources of  $N_2O$  were investigated by restricting the Keeling plot analysis for the absolute salinity/potential temperature ranges characteristic of AAIW as described in section 3.1. The analysis was restricted to 60°S to 20°S, even if the northernmost extent of AAIW is found below the ETNP, to eliminate possible effects of the ETNP and ETSP ODZs on  $N_2O$  production in this water mass.

$\Delta N_2O$  clearly increased from  $-0.89 \text{ nmol kg}^{-1}$  (-7.4% supersaturation) at 52°S to up to  $20.6 \text{ nmol kg}^{-1}$  (180% supersaturation) in the intermediate water mass AAIW (Figure 5), which is comparable to values observed by Carrasco et al. (2017). Keeling plot analysis revealed a  $N_2O$  source with a  $\delta^{15}N^{\text{bulk}} = 9.4\%$ ,  $\delta^{15}N^\alpha = 18.1\%$ ,  $\delta^{15}N^\beta = 0.8\%$ ,  $\delta^{18}O = 52.5\%$ , and SP = 17.2‰ (Table 1). The relatively high SP suggests that  $N_2O$  is mainly derived from nitrification, consistent with previous studies (Casciotti et al., 2018; Toyoda et al., 2019; Kelly et al., 2021). The positive significant relationship observed between  $\Delta N_2O$  and AOU in the AAIW water mass observed in this study and Carrasco et al. (2017) further supports this interpretation (Supplementary materials, Figure S2). The lower  $\delta^{15}N^\beta$  and higher  $\delta^{18}O$  and SP might reflect the influence of  $N_2O$  consumption in the ODZs in these prior studies.

## 4.3 Isotopic signatures of $N_2O$ consumption in the ETNP

High values of  $\delta^{15}N^\alpha$ ,  $\delta^{18}O$  and SP and low or negative  $\Delta N_2O$  were observed at  $[O_2] < 5 \text{ } \mu\text{mol kg}^{-1}$  in the ETNP ODZ, which are clear signatures of  $N_2O$  consumption (Figure 5). During  $N_2O$  reduction to  $N_2$  gas, the N-O bond is broken, leaving the remaining substrate ( $N_2O$ ) enriched in  $^{15}N$  and  $^{18}O$ . The  $\alpha$  position in  $N_2O$  is preferentially enriched in  $^{15}N$  compared to the  $\beta$  position since it is directly attached to the O atom being cleaved (e.g., Popp et al., 2002; Toyoda et al., 2002). Thus,  $\epsilon$  for the  $\alpha$  N atom (6.6–9.1‰) and  $\delta^{18}O$  (10.9–15‰) are relatively large with only a small or negligible  $\epsilon$  for  $\beta$  N atom (Ostrom et al., 2007). Notably, while  $\delta^{15}N^\alpha$  and  $\delta^{18}O$  increased in the ODZ,  $\delta^{15}N^\beta$  generally decreased, as also observed in previous ETNP and ETSP ODZ studies (Bourbonnais et al., 2017; Casciotti et al., 2018; Kelly et al., 2021) (Figure 5). This trend is not expected during pure  $N_2O$  consumption.

The slope for the relationship between  $\delta^{18}O$  versus and  $\delta^{15}N^\alpha$  ( $1.6 \pm 0.1$ ) was indistinguishable from the expected slope (i.e., 1.7) during  $N_2O$  consumption in soils and pure denitrifier cultures (Ostrom et al., 2007). However, the observed slope for  $\delta^{18}O$ - $N_2O$  versus SP ( $0.8 \pm 0.1$ ) clearly deviated from the expected value of 2.2 for pure  $N_2O$  reduction (Ostrom et al., 2007) (Figure 10). A wider

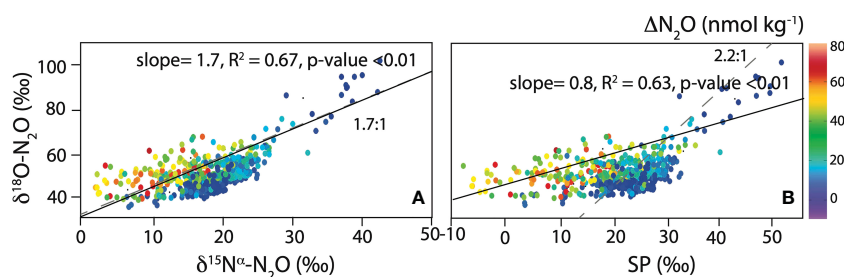


FIGURE 10  
 $\delta^{18}O$ - $N_2O$  versus (A)  $\delta^{15}N^\alpha$ - $N_2O$ , and (B) SP. The slope expected for pure denitrification is indicated with dashed grey lines (Ostrom et al., 2007).  $\Delta N_2O$  concentrations are shown as the color of the symbols (see color bar in top panel). Linear regressions for  $O_2 < 5 \text{ } \mu\text{mol kg}^{-1}$  are shown with black lines.

range of 1.3-3.3 for  $\delta^{18}\text{O}$  versus SP during consumption by denitrification was also reported for soil mesocosms, which is still higher than the slope observed in this study (Lewicka-Szczepak et al., 2017). This observation is consistent with previous studies in marine ODZs, reporting slopes for  $\delta^{18}\text{O}$  versus SP ranging between (0.9-1.8) (Bourbonnais et al., 2017; Casciotti et al., 2018; Kelly et al., 2021). For instance, in the ODZ off Peru, the slope for increase in  $\delta^{18}\text{O}$ - $\text{N}_2\text{O}$  versus SP deviates from what is expected during pure denitrification, mostly due to a decrease in  $\delta^{15}\text{N}^\beta$  within the ODZ (Bourbonnais et al., 2017; Casciotti et al., 2018). This trend showing a decreasing  $\delta^{15}\text{N}^\beta$  associated with high  $\delta^{18}\text{O}$ - $\text{N}_2\text{O}$  has also been observed in other ODZs and marine anoxic environments (Yamagishi et al., 2005; Westley et al., 2006; Yamagishi et al.,

2007; Farías et al., 2009; Kelly et al., 2021). The cause for the decreasing  $\delta^{15}\text{N}^\beta$  in the ODZ will be further discussed below.

In this study, apparent isotope effects ( $\epsilon_{\text{app}}$ ) were derived for all isopycnal ranges within the ETNP ODZ at  $[\text{O}_2] < 5 \mu\text{mol kg}^{-1}$ , where  $\text{N}_2\text{O}$  consumption is known to occur (Dalsgaard et al., 2014). This approach was used in Casciotti et al. (2018) to further investigate if a decrease in  $\epsilon^{18}\text{O}$  or increase in  $\epsilon^{\text{SP}}$  could explain the deviation from the expected slope for  $\delta^{18}\text{O}$ - $\text{N}_2\text{O}$  versus SP during pure  $\text{N}_2\text{O}$  consumption in the ETNP ODZ. Apparent isotope effects calculated for all isopycnal ranges were 3.6‰ for  $^{15}\text{N}^{\text{bulk}}$ , 9.4‰ for  $^{15}\text{N}^\alpha$ , -2.3‰ for  $^{15}\text{N}^\beta$ , 12.0‰ for  $^{18}\text{O}$  and 11.7‰ for SP (Table 2 and Figure 11). The  $\epsilon_{\text{app}}$  for  $^{15}\text{N}^{\text{bulk}}$  was slightly lower than the range reported for pure culture by Ostrom et al. (2007). Yet, the

TABLE 2 Apparent isotope effects for  $\text{N}_2\text{O}$  consumption (in ‰) calculated using a closed system Rayleigh model for  $^{15}\text{N}^{\text{bulk}}$ ,  $^{15}\text{N}^\alpha$ ,  $^{15}\text{N}^\beta$ ,  $^{18}\text{O}$  and SP for the ETNP.

	This study	Ostrom et al. (2007) Pure culture	Casciotti et al. (2018) ETNP ODZ	Kelly et al. (2021) ETNP ODZ
$\epsilon^{15}\text{N}^{\text{bulk}}$	$3.6 \pm 0.4$ $R^2 = 0.65, P < 0.01$	4.1 – 6.6	na	na
$\epsilon^{15}\text{N}^\alpha$	$9.4 \pm 0.9$ $R^2 = 0.66, P < 0.01$	6.6 – 9.1	na	$11.8 \pm 2.5$
$\epsilon^{15}\text{N}^\beta$	$-2.3 \pm 0.6$ $R^2 = 0.20, P < 0.01$	1.6 – 2.2	na	$-2.0 \pm 2.0$
$\epsilon^{18}\text{O}$	$12.0 \pm 1.3$ $R^2 = 0.60, P < 0.01$	10.9 – 15.0	14.5 – 25.6	$20.2 \pm 6.1$
$\epsilon^{\text{SP}}$	$11.7 \pm 1.4$ $R^2 = 0.57, P < 0.01$	5.0 – 6.8	11.6 – 17.5	na
$\epsilon^{18}\text{O}/\epsilon^{15}\text{N}^{\text{bulk}}$	$3.4 \pm 0.5$ $R^2 = 0.91, P < 0.01$	$2.5 \pm 0.2$	na	na
$\epsilon^{18}\text{O}/\epsilon^{\text{SP}}$	$1.0 \pm 0.2$	2.2	0.9 – 1.5	na

Only samples with  $[\text{O}_2] < 5 \mu\text{mol kg}^{-1}$  were considered. Isotope effects observed in pure laboratory culture and field studies in the ETNP and ETSP ODZs are also listed (Ostrom et al., 2007; Casciotti et al., 2018; Kelly et al., 2021). Standard error of the slope is shown. na means non available.

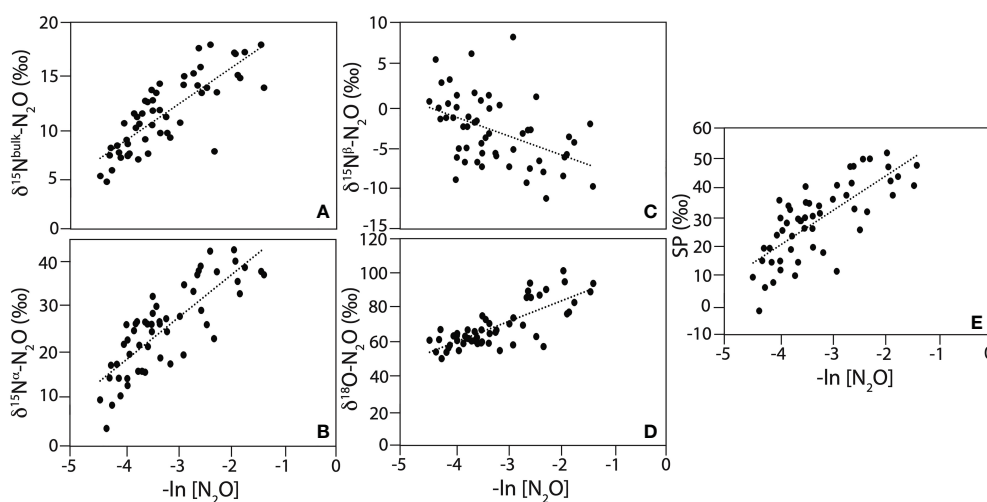


FIGURE 11

Apparent isotope effects for (A)  $\delta^{15}\text{N}^{\text{bulk}}\text{-N}_2\text{O}$ , (B)  $\delta^{15}\text{N}^\alpha\text{-N}_2\text{O}$ , (C)  $\delta^{15}\text{N}^\beta\text{-N}_2\text{O}$ , (D)  $\delta^{18}\text{O}\text{-N}_2\text{O}$ , and (E) SP calculated for  $[\text{O}_2] < 5 \mu\text{mol kg}^{-1}$ . Black lines are linear regressions. Linear regression outputs are reported in Table 2.

$\epsilon_{\text{app}}$  for  $^{15}\text{N}^{\alpha}$  and  $^{15}\text{N}^{\beta}$  were comparable to values (11.8‰ and -2‰, respectively) estimated by Kelly et al. (2021) in the ETNP ODZ. Notably, the negative isotope effect for  $^{15}\text{N}^{\beta}$  indicates a decrease in  $\delta^{15}\text{N}^{\beta}$  as  $\text{N}_2\text{O}$  is reduced to  $\text{N}_2$  within the ODZ. The  $\epsilon$  for  $^{18}\text{O}$  calculated in this study was significantly lower than the values (14.5 – 20.2‰) estimated in other ODZ marine field studies (Casciotti et al., 2018; Kelly et al., 2021), but comprised within the range observed for pure culture (10.9 – 15‰) (Ostrom et al., 2007). The  $\epsilon$  for SP was higher than for pure culture (5.0 – 6.8‰) but comparable to values estimated in the ETSP ODZ (11.6 – 17.5‰) (Casciotti et al., 2018). Casciotti et al. (2018) observed different apparent isotope effects at different isopycnal ranges within the ETSP ODZ. They observed a decrease in the  $\epsilon^{18}\text{O}$  within the ODZ (from 25.6‰ in the upper, to 19.6‰ in the middle and 14.5‰ in the lower ODZ) while the  $\epsilon\text{SP}$  increased slightly and then decreased (17.5‰ in the upper to 21.7‰ in the middle to 11.6‰ in the lower ODZ). A more detailed analysis by isopycnal ranges (upper, middle, and lower ODZ) could however not reproduce observed trends in Casciotti et al. (2018) for the P18 transect. For instance,  $\epsilon_{\text{app}}$  for  $^{18}\text{O}$  (13.9‰ in the upper ODZ to 11.4‰ in the middle, and 16.2‰ in the lower ODZ) and SP (14.2‰ in the upper ODZ to 7.5‰ in the middle, and 17.9‰ in the lower ODZ) both decreased toward the middle ODZ and then increased in the deeper ODZ (Supplementary materials, Figure S5). The slope for  $\epsilon^{18}\text{O}$  versus  $\epsilon\text{SP}$  also gradually decreased from 1.6 to 0.65 instead of being lowest in the middle ODZ. Irrespective of the observed trends, using a modeling approach and isotope values of substrates ( $\text{NO}_3^-$  and  $\text{N}^{18}\text{O}_2^-$ ) during denitrification, previous studies attributed the lower  $\epsilon^{18}\text{O}:\epsilon\text{SP}$  to an increase in SP due to a decrease in  $\delta^{15}\text{N}^{\beta}$  rather than a decrease in  $\epsilon^{18}\text{O}$  or increase in  $\epsilon\text{SP}$  in both the ETNP and ETSP ODZs (Casciotti et al., 2018; Kelly et al., 2021).

Several hypotheses have been proposed to explain the decreasing  $\delta^{15}\text{N}^{\beta}$  in ODZ waters, including concurrent  $\text{N}_2\text{O}$  production *via* denitrification of  $\text{NO}_3^-$  with a site preference  $>0\%$  (Schmidt et al., 2004; Casciotti et al., 2018; Kelly et al., 2021). Rate experiments as well as prior stable abundance isotopic studies suggest concurrent  $\text{N}_2\text{O}$  production and consumption as well as a rapid  $\text{N}_2\text{O}$  turnover in the ODZ (Fariás et al., 2009; Babbín et al., 2015; Ji et al., 2015; Bourbonnais et al., 2017; Casciotti et al., 2018; Frey et al., 2020; Kelly et al., 2021). Casciotti et al. (2018) modeled  $\text{N}_2\text{O}$  cycling at steady-state in the ODZ using both  $\delta^{15}\text{N}$  and  $\delta^{18}\text{O}$  of substrate molecules ( $\text{NO}_2^-$  and  $\text{NO}_3^-$ ) during denitrification.  $\text{N}_2\text{O}$  isotopic signatures were only reproduced when  $\text{NO}_3^-$  was used as the substrate and implying a site preference  $>0\%$  (i.e., greater fractionation at the  $^{15}\text{N}^{\beta}$  position relative to the  $^{15}\text{N}^{\alpha}$ ) during  $\text{N}_2\text{O}$  production by denitrification. This suggests that an internal (rather than ambient) pool of  $\text{NO}_2^-$  is used during denitrification as further discussed in Casciotti et al. (2018). Accordingly, a relatively long residence time was estimated for ambient  $\text{NO}_2^-$  (in the order of months) in the primary  $\text{NO}_2^-$  maximum and low- $\text{O}_2$  waters based on rates of abiotic O isotope exchange between nitrite and water (Buchwald and Casciotti, 2013; Bourbonnais et al., 2015). In another modeling study, a non-steady-state  $\text{N}_2\text{O}$  cycling as well as an ambient  $\text{NO}_2^-$  substrate source (with a  $\delta^{15}\text{N}$  as low as -30‰) or a SP of  $\sim 25\%$  during concurrent  $\text{N}_2\text{O}$  production by denitrification were required to explain the observed low  $\delta^{15}\text{N}^{\beta}$

values in the ETNP ODZ (Kelly et al., 2021). The low  $\delta^{15}\text{N}^{\beta}$  of  $\text{N}_2\text{O}$  could also result from an alternate mechanism in the ODZ, such as  $\text{N}_2\text{O}$  production from AO archaea and bacteria, which is associated with a high SP (30–38‰; Sutka et al., 2003; Sutka et al., 2004; Frame and Casciotti, 2010; Santoro et al., 2011; Löscher et al., 2012). For instance, an archaeal AO isolated from ODZs (*Nitrosopumilus maritimus*) produced both  $\text{N}_2$  and  $\text{O}_2$  under dark anaerobic conditions, following a pathway that involves  $\text{N}_2\text{O}$  as an intermediate (Kraft et al., 2022). Yet,  $\text{N}_2\text{O}$  production rates from AO based on  $^{15}\text{N}$ -labeled experiments were relatively low (up to 0.1  $\text{nmol L}^{-1} \text{d}^{-1}$ ) and generally at least one order of magnitude lower than  $\text{N}_2\text{O}$  production rates from  $\text{NO}_3^-$  (denitrification) under anoxic conditions in the ETSP ODZ (Frey et al., 2020).

The idea of denitrification with a site preference  $>0\%$  is not new (i.e., see Schmidt et al., 2004). Several studies invoked  $\text{N}_2\text{O}$  production during denitrification with a site preference  $>0\%$  in the ETNP and ETSP ODZs and Canadian Arctic bottom waters influenced by sedimentary processes (Casciotti et al., 2018; Lehmann et al., 2019; Kelly et al., 2021). Some variability in the SP of  $\text{N}_2\text{O}$  produced by denitrification was reported for different bacterial strains. For instance, Toyoda et al. (2005) observed a high SP of 22 to 24‰ for  $\text{N}_2\text{O}$  production during denitrification by *Pseudomonas fluorescens*, suggesting a symmetrical intermediate (i.e., *cis* formation mechanism). These observations for denitrifying bacteria are analogous to the wide range of SPs (15.8 – 37.1‰) that have been reported for different fungal species and strains (Maeda et al., 2015; Lazo-Murphy et al., 2022). These data challenge the conventional view that fungal denitrification fits into narrow compositional fields with relatively high SP values. Similarly, it is possible that denitrifying microbial consortia thriving under different  $\text{O}_2$  regimes are associated with variable SPs, but this hypothesis remains to be verified.

## 5 Concluding remarks

This study presents oceanic  $\text{N}_2\text{O}$  concentration, stable isotope and isotopomer data of unprecedentedly high spatial resolution along the P18 line in the eastern Pacific sampled in 2016/2017. Highest  $\Delta\text{N}_2\text{O}$  accumulations (up to 940% supersaturation) were observed close to the oxycline in both the ETNP and the fringe of the ETSP ODZ.  $\text{N}_2\text{O}$  yield from AOU increased at lower  $[\text{O}_2]$ , consistent with previous studies. Keeling plot analysis identified two distinct sources of  $\text{N}_2\text{O}$  at different  $[\text{O}_2]$  regimes. At lower  $[\text{O}_2]$  concentrations close to the oxycline in both ODZs, where highest  $\Delta\text{N}_2\text{O}$  were observed, SP of source  $\text{N}_2\text{O}$  was relatively low, suggesting production from denitrification (or nitrifier-denitrification). Relationships between  $\Delta\text{N}_2\text{O}$  and DIN deficit and the isotopic composition of  $\delta^{15}\text{N}$  of the substrate ( $\text{NO}_3^-$ ) further suggest that denitrification is the dominant process at low  $[\text{O}_2]$  concentrations. SP generally increased in more oxygenated surface waters, suggesting a greater contribution from nitrification. The isotopic composition of source  $\text{N}_2\text{O}$  in deeper waters of the ETNP and ETSP as well as in AAIW also suggested that nitrification was the main pathway for  $\text{N}_2\text{O}$  formation.

The  $\delta^{18}\text{O}$  versus  $\delta^{15}\text{N}^{\alpha}$  relationship showed a slope characteristic of  $\text{N}_2\text{O}$  consumption during denitrification in low  $\text{O}_2$  waters. Isotope

effects calculated for N<sub>2</sub>O consumption were consistent with previous field and laboratory studies (Ostrom et al., 2007; Casciotti et al., 2018; Kelly et al., 2021). Yet,  $\delta^{15}\text{N}^{\beta}$  decreased (rather than the predicted no change or slight increase during denitrification) in the ODZ, which was also observed by previous studies (e.g., Bourbonnais et al., 2017; Casciotti et al., 2018; and Kelly et al., 2021). These signatures are best explained by concurrent N<sub>2</sub>O production (from NO<sub>3</sub><sup>-</sup> or NO<sub>2</sub><sup>-</sup>) with a site preference >0‰, an ambient NO<sub>2</sub><sup>-</sup> source with a low  $\delta^{15}\text{N}$  and non-steady-state conditions (e.g., Kelly et al., 2021). Clearly, more research is needed to elucidate the SP and its variability for diverse denitrifying bacterial strains living in marine ODZs as current values are mostly from terrestrial environments (e.g., Toyoda et al., 2005). Some contribution from an alternative N<sub>2</sub>O production pathway is also possible, for example anaerobic AO (see Kraft et al., 2022).

This study establishes a benchmark against which to evaluate changes in N<sub>2</sub>O cycling for future decadal occupations of the P18 line. ODZs are currently expanding (Stramma et al., 2013), with unknown impacts on N<sub>2</sub>O cycling. The vertical expansion of ODZs not only increases the volume of low-O<sub>2</sub> waters where N<sub>2</sub>O is potentially produced but also increases N<sub>2</sub>O exchange with the atmosphere. However, co-occurring warming causes stronger stratification, which could reduce mixing and N<sub>2</sub>O outgassing to the atmosphere. At this point, it is unclear which mechanism will dominate. Thus, more observational data is needed to evaluate the impacts of ODZs expansion on marine N<sub>2</sub>O cycling and atmospheric emissions.

## Data availability statement

The datasets presented in this study can be found in online repositories. The names of the repository/repositories and accession number(s) can be found below: <https://cchdo.ucsd.edu/cruise/33RO20161119>.

## Author contributions

AB, SD, and MA designed the study. AB analyzed stable isotope and isotopomer samples. BC analyzed N<sub>2</sub>O concentration and CFC/SF<sub>6</sub> samples and RS calculated the transit time distributions. AB wrote the manuscript with input from all co-authors. All authors contributed to the article and approved the submitted version.

## References

- Altabet, M. A. (1988). Variations in nitrogen isotopic composition between sinking and suspended particles: Implications for nitrogen cycling and particle transformation in the open ocean. *Deep Sea Res. Part A. Oceanographic Res. Papers* 35 (4), 535–554. doi: 10.1016/0198-0149(88)90130-6
- Altabet, M. A. (2001). Nitrogen isotopic evidence for micronutrient control of fractional NO<sub>3</sub><sup>-</sup> utilization in the equatorial pacific. *Limnol. Oceanogr.* 46 (2), 368–380. doi: 10.4319/lo.2001.46.2.0368
- Altabet, M. A. (2006). "Isotopic tracers of the marine nitrogen cycle: present and past," in *Marine organic matter: Chemical and biological markers. the handbook of environmental chemistry*. Ed. J. Volkman (Berlin: Springer-Verlag), pp251–pp293.
- Altabet, M. A., Pilskaln, C., Thunell, R., Pride, C., Sigman, D., Chavez, F., et al. (1999). The nitrogen isotope biogeochemistry of sinking particles from the margin of

## Funding

This study was funded through a GO-SHIP National Science Foundation (NSF) postdoctoral Fellowship to AB (NSF OCE-1437015) and NSF OCE-2023545 that covered publication costs. MA and SD acknowledge support from NSF (OCE-1851361 and OCE-1947822). BC and RS were supported by the National Oceanic and Atmospheric Administration's Global Ocean Monitoring and Observations program.

## Acknowledgments

We thank the captain and crew of the NOAA R/V Ronald Brown for their support during the P18 research expedition. We also thank the scientific party, especially Brendan Carter, chief scientist during leg 1 of P18 and Alexander Sidelev for collecting N<sub>2</sub>O stable isotope and isotopomer samples during leg 2.

## Conflict of interest

The authors declare that the research was conducted in the absence of any commercial or financial relationships that could be construed as a potential conflict of interest.

## Publisher's note

All claims expressed in this article are solely those of the authors and do not necessarily represent those of their affiliated organizations, or those of the publisher, the editors and the reviewers. Any product that may be evaluated in this article, or claim that may be made by its manufacturer, is not guaranteed or endorsed by the publisher.

## Supplementary material

The Supplementary Material for this article can be found online at: <https://www.frontiersin.org/articles/10.3389/fmars.2023.1137064/full#supplementary-material>

the Eastern north pacific. *Deep Sea Res. Part I: Oceanographic Res. Papers* 46 (4), 655–679. doi: 10.1016/S0967-0637(98)00084-3

Altabet, M. A., Wassenaar, L. I., Douence, C., and Roy, R. (2019). A Ti (III) reduction method for one-step conversion of seawater and freshwater nitrate into N<sub>2</sub>O for stable isotopic analysis of <sup>15</sup>N/<sup>14</sup>N, <sup>18</sup>O/<sup>16</sup>O and <sup>17</sup>O/<sup>16</sup>O. *Rapid Commun. Mass Spectrometry* 33 (15), 1227–1239. doi: 10.1002/rcm.8454

Arévalo-Martínez, D. L., Kock, A., Löscher, C. R., Schmitz, R. A., and Bange, H. W. (2015). Massive nitrous oxide emissions from the tropical south pacific ocean. *Nat. Geosci.* 8 (7), 530–533. doi: 10.1038/ngeo2469

Arévalo-Martínez, D. L., Kock, A., Löscher, C. R., Schmitz, R. A., Stramma, L., and Bange, H. W. (2016). Influence of mesoscale eddies on the distribution of nitrous oxide in the eastern tropical south pacific. *Biogeosciences* 13 (4), 1105–1118. doi: 10.5194/bg-13-1105-2016

- Babbin, A. R., Bianchi, D., Jayakumar, A., and Ward, B. B. (2015). Rapid nitrous oxide cycling in the suboxic ocean. *Science* 348 (6239), 1127–1129. doi: 10.1126/science.aaa8380
- Babbin, A. R., Boles, E. L., Mühle, J., and Weiss, R. F. (2020). On the natural spatio-temporal heterogeneity of south pacific nitrous oxide. *Nat. Commun.* 11 (1), 1–9. doi: 10.1038/s41467-020-17509-6
- Bakker, D. C., Bange, H. W., Gruber, N., Johannessen, T., Upstill-Goddard, R. C., Borges, A. V., et al. (2014). Air-sea interactions of natural long-lived greenhouse gases (CO<sub>2</sub>, N<sub>2</sub>O, CH<sub>4</sub>) in a changing climate. *Ocean-Atmosphere Interactions of Gases and Particles*. (Switzerland AG: Springer Nature), pp113–169.
- Bange, H. W., Andreae, M. O., Lal, S., Law, C. S., Naqvi, S. W. A., Patra, P. K., et al. (2001). Nitrous oxide emissions from the Arabian Sea: A synthesis. *Atmospheric Chem. Phys.* 1 (1), 61–71. doi: 10.5194/acp-1-61-2001
- Barford, C. C., Montoya, J. P., Altabet, M. A., and Mitchell, R. (1999). Steady-state nitrogen isotope effects of N<sub>2</sub> and N<sub>2</sub>O production in paracoccus denitrificans. *Appl. Environ. Microbiol.* 65 (3), 989–994. doi: 10.1128/AEM.65.3.989-994.1999
- Berelson, W. M., Haskell, W. Z.II, Prokopenko, M., Knapp, A. N., Hammond, D. E., Rollins, N., et al. (2015). Biogenic particle flux and benthic remineralization in the Eastern tropical south pacific. *Deep Sea Res. Part I: Oceanographic Res. Papers* 99, 23–34. doi: 10.1016/j.dsr.2014.12.006
- Bourbonnais, A., Altabet, M. A., Charoenpong, C. N., Larkum, J., Hu, H., Bange, H. W., et al. (2015). N-loss isotope effects in the Peru oxygen minimum zone studied using a mesoscale eddy as a natural tracer experiment. *Global Biogeochemical Cycles* 29 (6), 793–811. doi: 10.1002/2014GB005001
- Bourbonnais, A., Lehmann, M. F., Wanick, J. J., and Schulz-Bull, D. E. (2009). Nitrate isotope anomalies reflect N<sub>2</sub> fixation in the Azores front region (subtropical NE Atlantic). *J. Geophys. Res.: Oceans* 114 (C3). doi: 10.1029/2007JC004617
- Bourbonnais, A., Letscher, R. T., Bange, H. W., Echevin, V., Larkum, J., Mohn, J., et al. (2017). N<sub>2</sub>O production and consumption from stable isotopic and concentration data in the Peruvian coastal upwelling system. *Global Biogeochemical Cycles* 31 (4), 678–698. doi: 10.1002/2016GB005567
- Bourbonnais, A., Frey, C., Sun, X., Bristow, L. A., Jayakumar, A., Ostrom, N. E., et al. (2021). Protocols for assessing transformation rates of nitrous oxide in the water column. *Front. Mar. Sci.* 8, 611937. doi: 10.3389/fmars.2021.611937
- Buchwald, C., and Casciotti, K. L. (2010). Oxygen isotopic fractionation and exchange during bacterial nitrite oxidation. *Limnol. Oceanogr.* 55 (3), 1064–1074. doi: 10.4319/lo.2010.55.3.1064
- Buchwald, C., and Casciotti, K. L. (2013). Isotopic ratios of nitrite as tracers of the sources and age of oceanic nitrite. *Nat. Geosci.* 6(4), 308–313.
- Caranto, J. D., and Lancaster, K. M. (2017). Nitric oxide is an obligate bacterial nitrification intermediate produced by hydroxylamine oxidoreductase. *Proc. Natl. Acad. Sci.* 114 (31), 8217–8222. doi: 10.1073/pnas.1704504114
- Carrasco, C., Karstensen, J., and Farias, L. (2017). On the nitrous oxide accumulation in intermediate waters of the eastern south pacific ocean. *Front. Mar. Sci.* 4, 24. doi: 10.3389/fmars.2017.00024
- Casciotti, K. L., Böhlke, J. K., McIlvin, M. R., Mroczkowski, S. J., and Hannon, J. E. (2007). Oxygen isotopes in nitrite: Analysis, calibration, and equilibration. *Analytical Chem.* 79 (6), 2427–2436. doi: 10.1021/ac061598h
- Casciotti, K. L., and Buchwald, C. (2012). Insights on the marine microbial nitrogen cycle from isotopic approaches to nitrification. *Front. Microbiol.* 3, 356. doi: 10.3389/fmicb.2012.00356
- Casciotti, K. L., Forbes, M., Vedamati, J., Peters, B. D., Martin, T. S., and Mordy, C. W. (2018). Nitrous oxide cycling in the Eastern tropical south pacific as inferred from isotopic and isotopomeric data. *Deep Sea Res. Part II: Topical Stud. Oceanogr.* 156, 155–167. doi: 10.1016/j.dsr2.2018.07.014
- Casciotti, K. L., Sigman, D. M., Hastings, M. G., Böhlke, J. K., and Hilkert, A. (2002). Measurement of the oxygen isotopic composition of nitrate in seawater and freshwater using the denitrifier method. *Analytical Chem.* 74 (19), 4905–4912. doi: 10.1021/ac020113w
- Chang, B. X., Devol, A. H., and Emerson, S. R. (2010). Denitrification and the nitrogen gas excess in the eastern tropical south pacific oxygen deficient zone. *Deep Sea Res. Part I: Oceanographic Res. Papers* 57 (9), 1092–1101. doi: 10.1016/j.dsr.2010.05.009
- Chang, B. X., Devol, A. H., and Emerson, S. R. (2012). Fixed nitrogen loss from the eastern tropical north pacific and Arabian Sea oxygen deficient zones determined from measurements of N<sub>2</sub>: Ar. *Global Biogeochem. Cycles* 26 (3). doi: 10.1029/2011GB004207
- Charoenpong, C. N., Bristow, L. A., and Altabet, M. A. (2014). A continuous flow isotope ratio mass spectrometry method for high precision determination of dissolved gas ratios and isotopic composition. *Limnol. Oceanogr.: Methods* 12 (5), 323–337. doi: 10.4319/lo.m.2014.12.323
- Ciais, P., Sabine, C., Bala, G., Bopp, L., Brovkin, V., Canadell, J., et al. (2013). Carbon and Other Biogeochemical Cycles. In: *Climate Change 2013: The Physical Science Basis. Contribution of Working Group I to the Fifth Assessment Report of the Intergovernmental Panel on Climate Change* [T. F. Stocker, D. Qin, G.-K. Plattner, M. Tignor, S. K. Allen, J. Boschung, et al (eds.)]. Cambridge University Press, Cambridge, United Kingdom and New York, NY, USA, pp465, pp570.
- Cline, J. D., and Kaplan, I. R. (1975). Isotopic fractionation of dissolved nitrate during denitrification in the eastern tropical north pacific ocean. *Mar. Chem.* 3 (4), 271–299. doi: 10.1016/0304-4203(75)90009-2
- Cohen, Y., and Gordon, L. I. (1979). Nitrous oxide production in the ocean. *J. Geophys. Res.: Oceans* 84 (C1), 347–353. doi: 10.1029/JC084iC01p0347
- Dalsgaard, T., Stewart, F. J., Thamdrup, B., De Brabandere, L., Revsbech, N. P., Ulloa, O., et al. (2014). Oxygen at nanomolar levels reversibly suppresses process rates and gene expression in anammox and denitrification in the oxygen minimum zone off northern Chile. *MBio* 5 (6), e01966–e01914. doi: 10.1128/mBio.01966-14
- Emery, W. J. (2001). Water types and water masses. *Encyclopedia ocean Sci.* 6, 3179–3187. doi: 10.1006/rwos.2001.0108
- Farias, L., Castro-González, M., Cornejo, M., Charpentier, J., Faúndez, J., Boontanon, N., et al. (2009). Denitrification and nitrous oxide cycling within the upper oxycline of the eastern tropical south pacific oxygen minimum zone. *Limnol. Oceanogr.* 54 (1), 132–144. doi: 10.4319/lo.2009.54.1.0132
- Forster, P., Storelmo, T., Armour, K., Collins, W., Dufresne, J.-L., Frame, D., et al. (2021). “The earth’s energy budget, climate feedbacks, and climate sensitivity,” in *Climate change 2021: The physical science basis. contribution of working group I to the sixth assessment report of the intergovernmental panel on climate change*. Eds. V. Masson-Delmotte, P. Zhai, A. Pirani, S. L. Connors, C. Péan, S. Berger, N. Caud, Y. Chen, L. Goldfarb, M. I. Gomis, M. Huang, K. Keitzell, E. Lonnoy, J. B. R. Matthews, T. K. Maycock, T. Waterfield, O. Yelekçi, R. Yu and B. Zhou (Cambridge, United Kingdom and New York, NY, USA: Cambridge University Press), pp923–p1054. doi: 10.1017/9781009157896.009
- Frame, C. H., and Casciotti, K. L. (2010). Biogeochemical controls and isotopic signatures of nitrous oxide production by a marine ammonia-oxidizing bacterium. *Biogeochemistry* 7 (9), 2695–2709. doi: 10.5194/bg-7-2695-2010
- Frame, C. H., Deal, E., Nevison, C. D., and Casciotti, K. L. (2014). N<sub>2</sub>O production in the eastern south Atlantic: Analysis of N<sub>2</sub>O stable isotopic and concentration data. *Global Biogeochemical Cycles* 28 (11), 1262–1278. doi: 10.1002/2013GB004790
- Frame, C. H., Lau, E., Nolan, E. J.IV, Goepfert, T. J., and Lehmann, M. F. (2017). Acidification enhances hybrid N<sub>2</sub>O production associated with aquatic ammonia-oxidizing microorganisms. *Front. Microbiol.* 7, 2104. doi: 10.3389/fmicb.2016.02104
- Freing, A., Wallace, D. W., and Bange, H. W. (2012). Global oceanic production of nitrous oxide. *Philos. Trans. R. Soc. B: Biol. Sci.* 367 (1593), 1245–1255. doi: 10.1098/rstb.2011.0360
- Freing, A., Wallace, D. W. R., Tanhua, T., Walter, S., and Bange, H. W. (2009). North Atlantic production of nitrous oxide in the context of changing atmospheric levels. *Global Biogeochemical Cycles* 23, 13. doi: 10.1029/2009gb003472
- Frey, C., Bange, H. W., Achterberg, E. P., Jayakumar, A., Löscher, C. R., Arévalo-Martínez, D. L., et al. (2020). Regulation of nitrous oxide production in low-oxygen waters off the coast of Peru. *Biogeochemistry* 17 (8), 2263–2287. doi: 10.5194/bg-17-2263-2020
- Fujii, A., Toyoda, S., Yoshida, O., Watanabe, S., Sasaki, K. I., and Yoshida, N. (2013). Distribution of nitrous oxide dissolved in water masses in the eastern subtropical north pacific and its origin inferred from isotopomer analysis. *J. Oceanogr.* 69 (2), 147–157. doi: 10.1007/s10872-012-0162-4
- Goreau, T. J., Kaplan, W. A., Wofsy, S. C., McElroy, M. B., Valois, F. W., and Watson, S. W. (1980). Production of NO<sub>2</sub><sup>-</sup> and N<sub>2</sub>O by nitrifying bacteria at reduced concentrations of oxygen. *Appl. Environ. Microbiol.* 40 (3), 526–532. doi: 10.1128/aem.40.3.526-532.1980
- Granger, J., Sigman, D. M., Lehmann, M. F., and Tortell, P. D. (2008). Nitrogen and oxygen isotope fractionation during dissimilatory nitrate reduction by denitrifying bacteria. *Limnol. Oceanogr.* 53 (6), 2533–2545. doi: 10.4319/lo.2008.53.6.2533
- Granger, J., Sigman, D. M., Needoba, J. A., and Harrison, P. J. (2004). Coupled nitrogen and oxygen isotope fractionation of nitrate during assimilation by cultures of marine phytoplankton. *Limnol. Oceanogr.* 49 (5), 1763–1773. doi: 10.4319/lo.2004.49.5.1763
- Heil, J., Wolf, B., Brüggemann, N., Emmenegger, L., Tuzson, B., Vereecken, H., et al. (2014). Site-specific <sup>15</sup>N isotopic signatures of abiotically produced N<sub>2</sub>O. *Geochimica Cosmochimica Acta* 139, 72–82. doi: 10.1016/j.gca.2014.04.037
- Hink, L., Lycus, P., Gubry-Rangin, C., Frostegård, Å., Nicol, G. W., Prosser, J. I., et al. (2017a). Kinetics of NH<sub>3</sub>-oxidation, NO<sub>2</sub>-turnover, N<sub>2</sub>O-production and electron flow during oxygen depletion in model bacterial and archaeal ammonia oxidisers. *Environ. Microbiol.* 19 (12), 4882–4896. doi: 10.1111/1462-2920.13914
- Hink, L., Nicol, G. W., and Prosser, J. I. (2017b). Archaea produce lower yields of N<sub>2</sub>O than bacteria during aerobic ammonia oxidation in soil. *Environ. Microbiol.* 19 (12), 4829–4837.
- Howell, E. A., Doney, S. C., Fine, R. A., and Olson, D. B. (1997). Geochemical estimates of denitrification rates for the Arabian Sea and bay of Bengal during WOCE. *Geophys. Res. Lett.* 24, 2549–2552. doi: 10.1029/97GL01538
- Ji, Q., Altabet, M. A., Bange, H. W., Graco, M. I., Ma, X., Arévalo-Martínez, D. L., et al. (2019). Investigating the effect of El Niño on nitrous oxide distribution in the eastern tropical south pacific. *Biogeochemistry* 16 (9), 2079–2093. doi: 10.5194/bg-16-2079-2019
- Ji, Q., Babbin, A. R., Jayakumar, A., Oleynik, S., and Ward, B. B. (2015). Nitrous oxide production by nitrification and denitrification in the Eastern tropical south pacific oxygen minimum zone. *Geophys. Res. Lett.* 42 (24), 10–755. doi: 10.1002/2015GL066853
- Ji, Q., Buitenhuis, E., Suntharalingam, P., Sarmiento, J. L., and Ward, B. B. (2018). Global nitrous oxide production determined by oxygen sensitivity of nitrification and

- denitrification. *Global Biogeochemical Cycles* 32 (12), 1790–1802. doi: 10.1029/2018GB005887
- Keeling, C. D. (1961). The concentration and isotopic abundances of carbon dioxide in rural and marine air. *Geochimica Cosmochimica Acta* 24 (3-4), 277–298. doi: 10.1016/0016-7037(61)90023-0
- Kelly, C. L., Travis, N. M., Baya, P. A., and Casciotti, K. L. (2021). Quantifying nitrous oxide cycling regimes in the Eastern tropical north pacific ocean with isotopomer analysis. *Global Biogeochemical Cycles* 35 (2), e2020GB006637. doi: 10.1029/2020GB006637
- Kock, A., Arévalo-Martínez, D. L., Löscher, C. R., and Bange, H. W. (2016). Extreme N<sub>2</sub>O accumulation in the coastal oxygen minimum zone off Peru. *Biogeosciences* 13 (3), 827–840. doi: 10.5194/bg-13-827-2016
- Kool, D. M., Dolfing, J., Wrage, N., and Van Groenigen, J. W. (2011). Nitrifier denitrification as a distinct and significant source of nitrous oxide from soil. *Soil Biol. Biochem.* 43 (1), 174–178. doi: 10.1016/j.soilbio.2010.09.030
- Kozłowski, J. A., Stieglmeier, M., Schleper, C., Klotz, M. G., and Stein, L. Y. (2016). Pathways and key intermediates required for obligate aerobic ammonia-dependent chemolithotrophy in bacteria and thaumarchaeota. *ISME J.* 10 (8), 1836–1845. doi: 10.1038/ismej.2016.2
- Kraft, B., Jehmlich, N., Larsen, M., Bristow, L. A., Könneke, M., Thamdrup, B., et al. (2022). Oxygen and nitrogen production by an ammonia-oxidizing archaeon. *Science* 375 (6576), 97–100. doi: 10.1126/science.abe6733
- Lazo-Murphy, B. M., Larson, S., Staines, S., Bruck, H., McHenry, J., Bourbonnais, A., et al. (2022). Nitrous oxide production and isotopomer composition by fungi isolated from salt marsh sediments. *Front. Mar. Sci.* 9, 2645. doi: 10.3389/fmars.2022.1098508
- Lehmann, N., Kienast, M., Granger, J., Bourbonnais, A., Altabet, M. A., and Tremblay, J.É. (2019). Remote western Arctic nutrients fuel remineralization in deep Baffin bay. *Global Biogeochemical Cycles* 33 (6), 649–667. doi: 10.1029/2018GB006134
- Lewicka-Szczepak, D., Augustin, J., Giesemann, A., and Well, R. (2017). Quantifying N<sub>2</sub>O reduction to N<sub>2</sub> based on N<sub>2</sub>O isotopocules—validation with independent methods (helium incubation and <sup>15</sup>N gas flux method). *Biogeosciences* 14 (3), 711–732. doi: 10.5194/bg-14-711-2017
- Löscher, C. R., Kock, A., Könneke, M., LaRoche, J., Bange, H. W., and Schmitz, R. A. (2012). Production of oceanic nitrous oxide by ammonia-oxidizing archaea. *Biogeosciences* 9 (7), 2419–2429. doi: 10.5194/bg-9-2419-2012
- Maeda, K., Spor, A., Edel-Hermann, V., Heraud, C., Breuil, M. C., Bizouard, F., et al. (2015). N<sub>2</sub>O production, a widespread trait in fungi. *Sci. Rep.* 5 (1), 9697. doi: 10.1038/srep09697
- Magyar, P. M. (2017). *Insights into pathways of nitrous oxide generation from novel isotopologue measurements*. Dissertation (Ph.D.), California Institute of Technology, 119 pp. doi: 10.7907/Z93776RJ
- Mariotti, A., Germon, J. C., Hubert, P., Kaiser, P., Letolle, R., Tardieux, A., et al. (1981). Experimental determination of nitrogen kinetic isotope fractionation: some principles; illustration for the denitrification and nitrification processes. *Plant Soil* 62 (3), 413–430. doi: 10.1007/BF02374138
- Mohr, J., Wolf, B., Toyoda, S., Lin, C. T., Liang, M. C., Brüggemann, N., et al. (2014). Interlaboratory assessment of nitrous oxide isotopomer analysis by isotope ratio mass spectrometry and laser spectroscopy: current status and perspectives. *Rapid Commun. Mass Spectrometry* 28 (18), 1995–2007. doi: 10.1002/rcm.6982
- Monreal, P. J., Kelly, C. L., Travis, N. M., and Casciotti, K. L. (2022). Identifying the sources and drivers of nitrous oxide accumulation in the eddy-influenced Eastern tropical north pacific oxygen-deficient zone. *Glob. Biogeochem. Cycles* 36 (6), e2022GB007310. doi: 10.1007/BF02374138
- Muggeo, V. M. (2003). Estimating regression models with unknown break-points. *Stat. Med.* 22(19), 3055–3071. doi: 10.1002/sim.1545
- Muggeo, V. M., and Muggeo, M. V. M. (2017). Package ‘segmented’. *Biometrika* 58 (525-534), 516.
- Nevison, C., Butler, J. H., and Elkins, J. W. (2003). Global distribution of N<sub>2</sub>O and the ΔN<sub>2</sub>O-AOU yield in the subsurface ocean. *Global Biogeochemical Cycles* 17 (4). doi: 10.1029/2003GB002068
- Nevison, C., and Holland, E. (1997). A reexamination of the impact of anthropogenically fixed nitrogen on atmospheric N<sub>2</sub>O and the stratospheric O<sub>3</sub> layer. *J. Geophys. Res.: Atmospheres* 102 (D21), 25519–25536. doi: 10.1029/97JD02391
- Ostrom, N. E., and Ostrom, P. H. (2012). “The isotopomers of nitrous oxide: analytical considerations and application to resolution of microbial production pathways,” in *Handbook of environmental isotope geochemistry* (Berlin, Heidelberg: Springer), pp453–pp476. doi: 10.1029/2006JG000287
- Ostrom, N. E., Pitt, A., Sutka, R., Ostrom, P. H., Grandy, A. S., Huizinga, K. M., et al. (2007). Isotopologue effects during N<sub>2</sub>O reduction in soils and in pure cultures of denitrifiers. *J. Geophys. Res.: Biogeosciences* 112 (G2). doi: 10.1029/2006JG000287
- Pataki, D. E., Ehleringer, J. R., Flanagan, L. B., Yakir, D., Bowling, D. R., Still, C. J., et al. (2003). The application and interpretation of keeling plots in terrestrial carbon cycle research. *Global Biogeochem. Cycles* 17 (1). doi: 10.1029/2001GB001850
- Popp, B. N., Westley, M. B., Toyoda, S., Miwa, T., Dore, J. E., Yoshida, N., et al. (2002). Nitrogen and oxygen isotopomeric constraints on the origins and sea-to-air flux of N<sub>2</sub>O in the oligotrophic subtropical north pacific gyre. *Global Biogeochemical Cycles* 16 (4), 12–11. doi: 10.1029/2001GB001806
- Ravishankara, A. R., Daniel, J. S., and Portmann, R. W. (2009). Nitrous oxide (N<sub>2</sub>O): the dominant ozone-depleting substance emitted in the 21<sup>st</sup> century. *Science* 326 (5949), 123–125. doi: 10.1126/science.1176985
- Ryabenko, E., Kock, A., Bange, H. W., Altabet, M. A., and Wallace, D. W. R. (2012). Contrasting biogeochemistry of nitrogen in the Atlantic and pacific oxygen minimum zones. *Biogeosciences* 9, 203–215. doi: 10.5194/bg-9-203-2012
- Santoro, A. E., Buchwald, C., McIlvin, M. R., and Casciotti, K. L. (2011). Isotopic signature of N<sub>2</sub>O produced by marine ammonia-oxidizing archaea. *Science* 333 (6047), 1282–1285. doi: 10.1126/science.1208239
- Santoro, A. E., Casciotti, K. L., and Francis, C. A. (2010). Activity, abundance and diversity of nitrifying archaea and bacteria in the central California current. *Environ. Microbiol.* 12 (7), 1989–2006. doi: 10.1111/j.1462-2920.2010.02205.x
- Schmidt, H. L., Werner, R. A., Yoshida, N., and Well, R. (2004). Is the isotopic composition of nitrous oxide an indicator for its origin from nitrification or denitrification? a theoretical approach from referred data and microbiological and enzyme kinetic aspects. *Rapid Commun. Mass Spectrometry* 18 (18), 2036–2040. doi: 10.1002/rcm.1586
- Sigman, D. M., Granger, J., DiFiore, P. J., Lehmann, M. M., Ho, R., Cane, G., et al. (2005). Coupled nitrogen and oxygen isotope measurements of nitrate along the eastern north pacific margin. *Global Biogeochemical Cycles* 19 (4). doi: 10.1029/2005GB002458
- Snider, D. M., Venkiteswaran, J. J., Schiff, S. L., and Spoelstra, J. (2012). Deciphering the oxygen isotope composition of nitrous oxide produced by nitrification. *Global Change Biol.* 18 (1), 356–370. doi: 10.1111/j.1365-2486.2011.02547.x
- Sonnerup, R. E., Mecking, S., Bullister, J. L., and Warner, M. J. (2015). Transit time distributions and oxygen utilization rates from chlorofluorocarbons and sulfur hexafluoride in the southeast pacific ocean. *J. Geophys. Res. Ocean.* 120, doi:10.1002/2015JC010781. doi: 10.1002/2015JC010781
- Stanley, R. H. R., Doney, S. C., Jenkins, W. J., and Lott, D. E. (2012). Apparent oxygen utilization rates calculated from tritium and helium-3 profiles at the Bermuda Atlantic time-series study site. *Biogeosciences* 9 (6), 1969–1983. doi: 10.5194/bg-9-1969-2012
- Stieglmeier, M., Mooshammer, M., Kitzler, B., Wanek, W., Zechmeister-Boltenstern, S., Richter, A., et al. (2014). Aerobic nitrous oxide production through n-nitrosating hybrid formation in ammonia-oxidizing archaea. *ISME J.* 8 (5), 1135–1146. doi: 10.1038/ismej.2013.220
- Stöven, T., Tanhua, T., Hoppema, M., and Bullister, J. L. (2015). Perspectives of transient tracer applications and limiting cases. *Ocean Sci.* 11 (5), 699–718. doi: 10.5194/os-11-699-2015
- Stramma, L., Bange, H. W., Czeschel, R., Lorenzo, A., and Frank, M. (2013). On the role of mesoscale eddies for the biological productivity and biogeochemistry in the eastern tropical Pacific Ocean off Peru. *Biogeosciences* 10 (11), 7293–7306. doi: 10.5194/bg-10-7293-2013
- Sutka, R. L., Ostrom, N. E., Ostrom, P. H., Breznak, J. A., Gandhi, H., Pitt, A. J., et al. (2006). Distinguishing nitrous oxide production from nitrification and denitrification on the basis of isotopomer abundances. *Appl. Environ. Microbiol.* 72 (1), 638–644. doi: 10.1128/AEM.72.1.638-644.2006
- Sutka, R. L., Ostrom, N. E., Ostrom, P. H., Gandhi, H., and Breznak, J. A. (2003). Nitrogen isotopomer site preference of N<sub>2</sub>O produced by nitrosomonas europaea and methylcoccus capsulatus bath. *Rapid Commun. Mass Spectrometry* 17 (7), 738–745. doi: 10.1002/rcm.968
- Sutka, R. L., Ostrom, N. E., Ostrom, P. H., and Phanikumar, M. S. (2004). Stable nitrogen isotope dynamics of dissolved nitrate in a transect from the north pacific subtropical gyre to the Eastern tropical north pacific. *Geochimica Cosmochimica Acta* 68 (3), 517–527. doi: 10.1016/S0016-7037(03)00483-6
- Tian, H., Xu, R., Canadell, J. G., Thompson, R. L., Winiwarter, W., Suntharalingam, P., et al. (2020). A comprehensive quantification of global nitrous oxide sources and sinks. *Nature* 586, 248–256. doi: 10.1038/s41586-020-2780-0
- Toyoda, S., Mutobe, H., Yamagishi, H., Yoshida, N., and Tanji, Y. (2005). Fractionation of N<sub>2</sub>O isotopomers during production by denitrifier. *Soil Biol. Biochem.* 37 (8), 1535–1545. doi: 10.1016/j.soilbio.2005.01.009
- Toyoda, S., Yoshida, N., Miwa, T., Matsui, Y., Yamagishi, H., Tsunogai, U., et al. (2002). Production mechanism and global budget of N<sub>2</sub>O inferred from its isotopomers in the western north pacific. *Geophys. Res. Lett.* 29 (3), 7–1. doi: 10.1029/2001GL014311
- Toyoda, S., Yoshida, O., Yamagishi, H., Fujii, A., Yoshida, N., and Watanabe, S. (2019). Identifying the origin of nitrous oxide dissolved in deep ocean by concentration and isotopocule analyses. *Sci. Rep.* 9 (1), 1–9. doi: 10.1038/s41598-019-44224-0
- Trimmer, M., Chronopoulou, P. M., Maanoja, S. T., Upstill-Goddard, R. C., Kitudis, V., and Purdy, K. J. (2016). Nitrous oxide as a function of oxygen and archaeal gene abundance in the north pacific. *Nat. Commun.* 7 (1), 1–10. doi: 10.1038/ncomms13451
- Wankel, S. D., Ziebis, W., Buchwald, C., Charoenpong, C., de Beer, D., Dentinger, J., et al. (2017). Evidence for fungal and chemodenitrification based N<sub>2</sub>O flux from nitrogen impacted coastal sediments. *Nat. Commun.* 8 (1), 1–11. doi: 10.1038/ncomms15595
- Ward, B. B. (2008). “Nitrification in marine systems,” in *Nitrogen in the marine environment*. Eds. D. G. Capone, D. A. Bronk, M. R. Mulholland and E. J. Carpenter (Elsevier, San Diego, California: Academic Press), pp199–pp261.

- Waugh, D. W., Hall, T. M., and Haine, T. W. N. (2003). Relationships among tracer ages. *J. Geophys. Research-Oceans* 108 (C5), 16. doi: 10.1029/2002jc001325
- Weiss, R. F., and Price, B. A. (1980). Nitrous oxide solubility in water and seawater. *Mar. Chem.* 8 (4), 347–359. doi: 10.1016/0304-4203(80)90024-9
- Westley, M. B., Popp, B. N., and Rust, T. M. (2007). The calibration of the intramolecular nitrogen isotope distribution in nitrous oxide measured by isotope ratio mass spectrometry. *Rapid Commun. Mass Spectrometry* 21 (3), 391–405. doi: 10.1002/rcm.2828
- Westley, M. B., Yamagishi, H., Popp, B. N., and Yoshida, N. (2006). Nitrous oxide cycling in the black Sea inferred from stable isotope and isotopomer distributions. *Deep Sea Res. Part II: Topical Stud. Oceanogr.* 53, 1802–1816. doi: 10.1016/j.dsr2.2006.03.012
- Wrage, N., Velthof, G. L., Van Beusichem, M. L., and Oenema, O. (2001). Role of nitrifier denitrification in the production of nitrous oxide. *Soil Biol. Biochem.* 33 (12–13), 1723–1732. doi: 10.1016/S0038-0717(01)00096-7
- Yamagishi, H., Westley, M. B., Popp, B. N., Toyoda, S., Yoshida, N., Watanabe, S., et al. (2007). Role of nitrification and denitrification on the nitrous oxide cycle in the eastern tropical north pacific and gulf of California. *J. Geophys. Res.: Biogeosciences* 112 (G2). doi: 10.1029/2006JG000227
- Yamagishi, H., Yoshida, N., Toyoda, S., Popp, B. N., Westley, M. B., and Watanabe, S. (2005). Contributions of denitrification and mixing on the distribution of nitrous oxide in the north pacific. *Geophys. Res. Lett.* 32 (4). doi: 10.1029/2004GL021458
- Yang, S., Chang, B. X., Warner, M. J., Weber, T. S., Bourbonnais, A. M., Santoro, A. E., et al. (2020). Global reconstruction reduces the uncertainty of oceanic nitrous oxide emissions and reveals a vigorous seasonal cycle. *Proc. Natl. Acad. Sci.* 117 (22), 11954–11960. doi: 10.1073/pnas.1921914117
- Yoshida, N., Morimoto, H., Hirano, M., Koike, I., Matsuo, S., Wada, E., et al. (1989). Nitrification rates and <sup>15</sup>N abundances of N<sub>2</sub>O and NO<sub>3</sub> in the western north pacific. *Nature* 342 (6252), 895–897.
- Yoshinari, T., and Knowles, R. (1976). Acetylene inhibition of nitrous oxide reduction by denitrifying bacteria. *Biochem. Biophys. Res. Commun.* 69 (3), 705–710. doi: 10.1016/0006-291X(76)90932-3